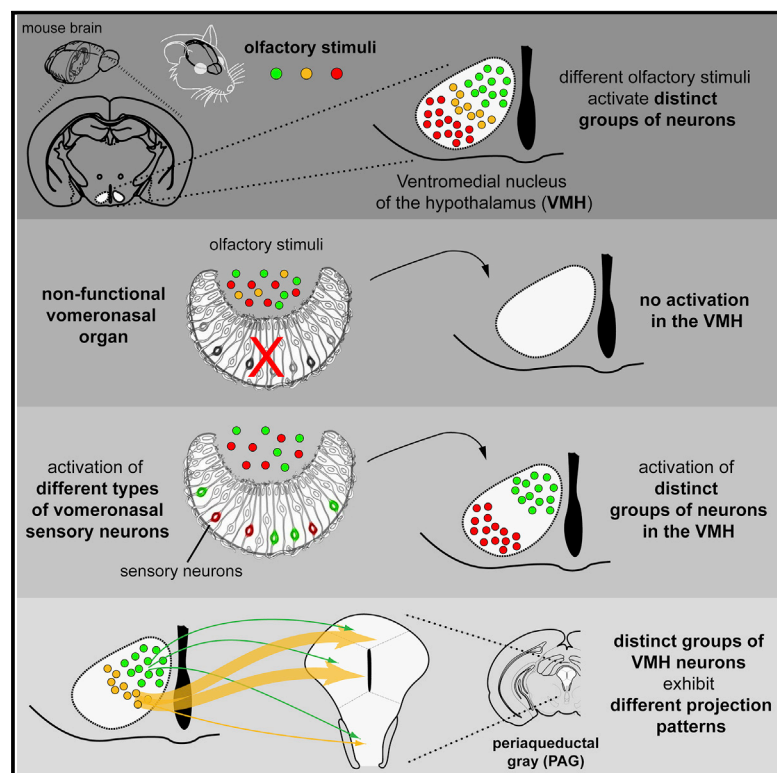


Representation of Olfactory Information in Organized Active Neural Ensembles in the Hypothalamus

Graphical Abstract



Highlights

- Different stimuli lead to distinct spatial patterns of active VMH neurons
- Representation of olfactory information in the VMH is dependent on vomeronasal input
- Activated vomeronasal receptors correlate with the location of active VMH ensembles
- Distinct VMH ensembles are associated with different output projection patterns

Authors

Vinicius Miessler de Andrade Carvalho, Thiago Seike Nakahara, Mateus Augusto de Andrade Souza, ..., José Otávio Venancio, Lisa Stowers, Fabio Papes

Correspondence

papesf@unicamp.br

In Brief

Carvalho et al. find that mice exposed to different odors display activation of distinctly located neurons in the ventromedial nucleus of the hypothalamus in the brain. The spatial location of activated neurons depends on the vomeronasal organ in the nose and correlates with its activated sensory receptors.



Report

Representation of Olfactory Information in Organized Active Neural Ensembles in the Hypothalamus

Vinicius Miessler de Andrade Carvalho,^{1,2,3} Thiago Seike Nakahara,^{1,2} Mateus Augusto de Andrade Souza,^{1,2} Leonardo Minete Cardozo,^{1,2} Guilherme Ziegler Trintinalia,^{1,2} Leonardo Granato Pissinato,^{1,2} José Otávio Venancio,¹ Lisa Stowers,³ and Fabio Papes^{1,4,*}

¹Department of Genetics, Evolution, Microbiology and Immunology, Institute of Biology, University of Campinas, Rua Monteiro Lobato, 255, Campinas, São Paulo 13083-862, Brazil

²Graduate Program in Genetics and Molecular Biology, Institute of Biology, University of Campinas, Rua Monteiro Lobato, 255, Campinas, São Paulo 13083-862, Brazil

³Department of Cell Biology, Scripps Research, 10550 N. Torrey Pines Rd., La Jolla, CA 92037, USA

⁴Lead Contact

*Correspondence: papesf@unicamp.br
<https://doi.org/10.1016/j.celrep.2020.108061>

SUMMARY

The internal representation of sensory information via coherent activation of specific pathways in the nervous system is key to appropriate behavioral responses. Little is known about how chemical stimuli that elicit instinctive behaviors lead to organized patterns of activity in the hypothalamus. Here, we study how a wide range of chemosignals form a discernible map of olfactory information in the ventromedial nucleus of the hypothalamus (VMH) and show that different stimuli entail distinct active neural ensembles. Importantly, we demonstrate that this map depends on functional inputs from the vomeronasal organ. We present evidence that the spatial locations of active VMH ensembles are correlated with activation of distinct vomeronasal receptors and that disjunct VMH ensembles exhibit differential projection patterns. Moreover, active ensembles with distinct spatial locations are not necessarily associated with different behavior categories, such as defensive or social, calling for a revision of the currently accepted model of VMH organization.

INTRODUCTION

Understanding how sensory information leads to organized patterns of neural activity is crucial to deciphering how the nervous system works to perceive and respond to the external world. Odorants have been shown to be represented in large sets of dispersed neurons in the piriform cortex (Ghosh et al., 2011; Miyamichi et al., 2011; Schaffer et al., 2018; Sosulski et al., 2011), but little is known of how instinctive behavior-inducing chemosignals are mapped in the brain.

Odors mediate a range of behavioral responses, such as aggression (Chamero et al., 2007), mating, gender discrimination (Kimchi et al., 2007; Stowers et al., 2002), and fear (Papes et al., 2010). These cues activate several brain areas, including the ventromedial nucleus of the hypothalamus (VMH), which has been functionally implicated with the generation of behavior (Hashikawa et al., 2017; Kunwar et al., 2015; Lee et al., 2014; Lin et al., 2011; Silva et al., 2013; Wang et al., 2015).

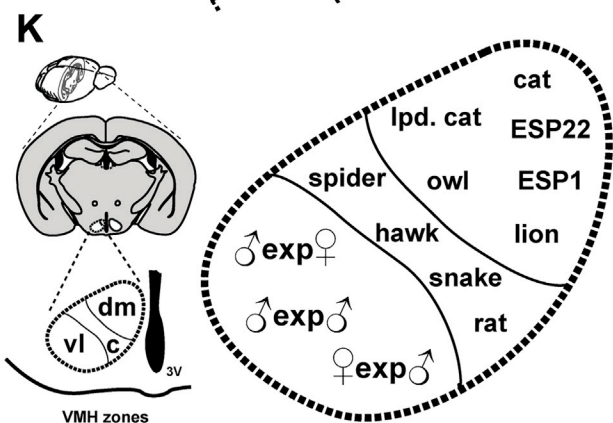
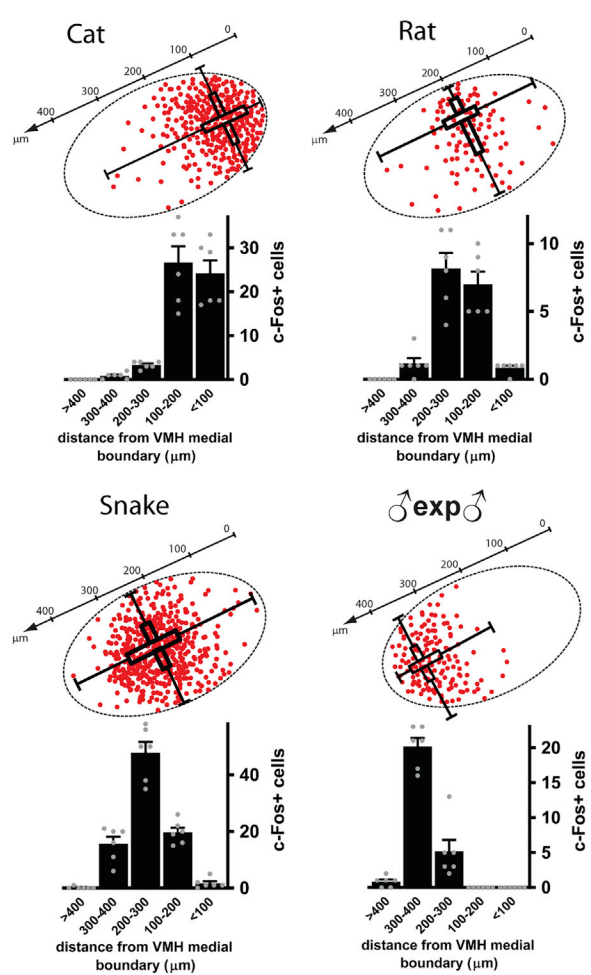
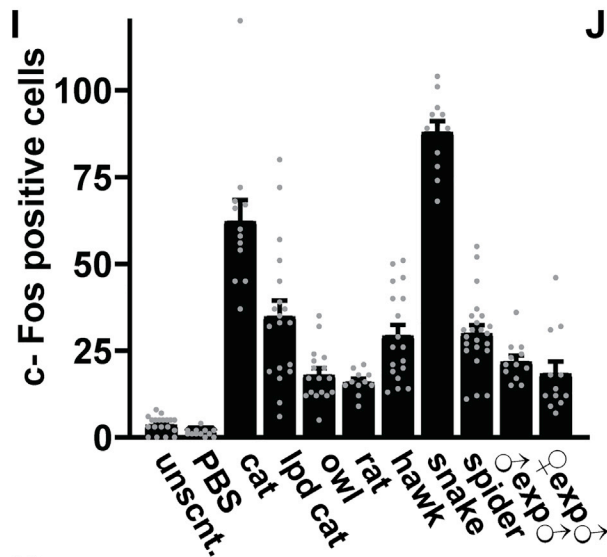
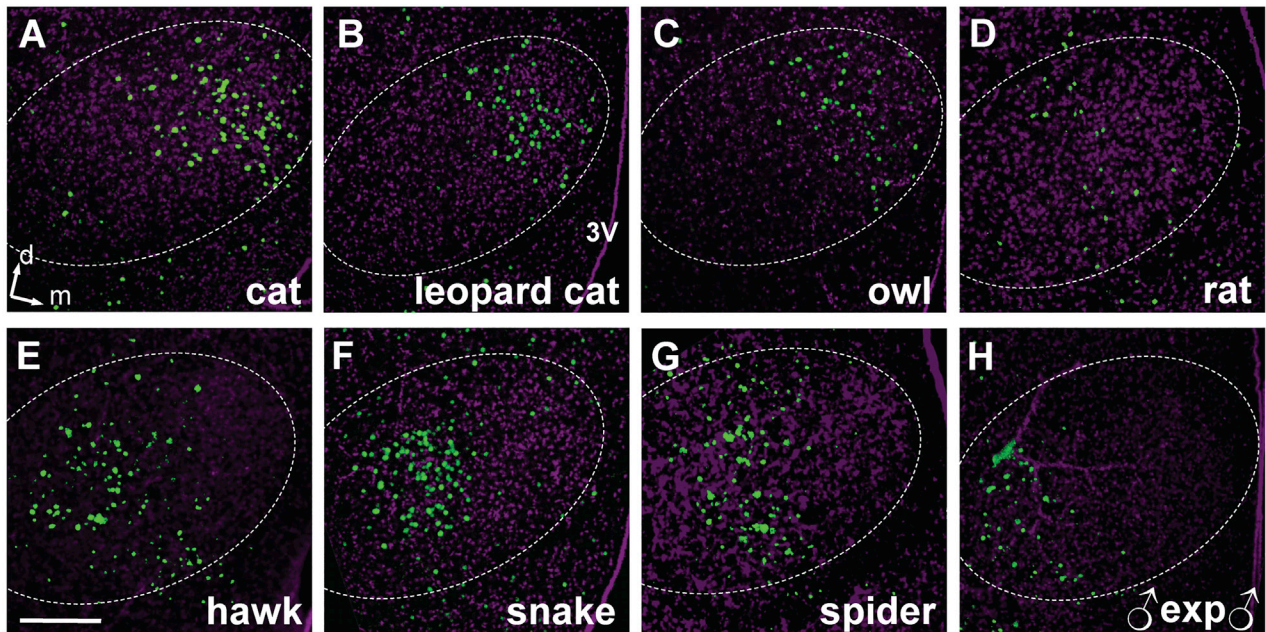
Conspecific odors that elicit social behaviors were found to activate neurons in the ventrolateral VMH (VMH_{vl}), whereas predator odors, which trigger defensive behavior, activate the dorsomedial VMH (VMH_{dm}) (Choi et al., 2005; Dielenberg et al., 2001). Optogenetic activation of VMH_{vl} triggered aggression (Lin et al.,

2011), and modulation of estrogen receptor alpha-expressing (Esr1⁺) VMH_{vl} neurons altered social behaviors (Lee et al., 2014; Silva et al., 2013). In contrast, functional manipulation of the VMH_{dm} showed that its steroidogenic-factor-1-expressing (SF1⁺) neurons command defensive behaviors (Kunwar et al., 2015; Silva et al., 2013; Wang et al., 2015).

These studies crystallized the notion that the VMH is separated into dorsomedial and ventrolateral sectors, devoted to defensive and social behaviors, respectively (Choi et al., 2005; Swanson, 2000). However, those ideas arose from studies that used a limited variety of stimuli. Recent reports have questioned the defensive-social separation (Ishii et al., 2017; Osakada et al., 2018) and have found that VMH activity is not invariant and may be shaped by experience (Remedios et al., 2017). This scenario is further complicated because each VMH sub-population exhibits hodological input convergence and output divergence (Kim et al., 2019; Lo et al., 2019), and a clear relationship between activity in distinct VMH cell types and specific behaviors could not be observed (Kim et al., 2019).

Therefore, the organization of olfactory information in the VMH remains to be fully elucidated. Here, we investigate VMH activity using a comprehensive repertoire of olfactory chemosignals and describe distinct stimuli activating differently positioned





(legend on next page)

ensembles in that nucleus. We show that such activity is dependent on a functional vomeronasal organ (VNO) and that the set of activated vomeronasal receptors for each stimulus correlates with the spatial location of the corresponding active VMH ensemble. Moreover, we provide evidence that spatially disjunct ensembles activated by distinct odors project differentially to the periaqueductal gray (PAG), an important effector brain region. Our results indicate the need for a revision of the simplified division of the VMH into defensive and social behavior zones.

RESULTS

Distinct Olfactory Stimuli Activate Spatially Segregated Groups of Neurons in the Ventromedial Hypothalamus

We exposed male mice to a comprehensive repertoire of behavior-inducing olfactory chemosignals (Table S1) to investigate the organization of VMH activity (Figures 1A–1I), revealing a range of different spatial patterns of activation that vary according to stimulus. Cat, leopard cat, and owl odors activated cells in the VMH_{dm}, as judged by c-Fos induction (Figures 1A–1C, 1J, and S1A). Rat, hawk, snake, and spider odors activated a more centrally located portion of the nucleus, VMH_c (Figures 1D–1G, 1J, and S1A). In contrast, we observed activity in the VMH_{vl} in mice exposed to some conspecific stimuli (Figures 1H, 1J, and S1D) (Choi et al., 2005; Dielenberg et al., 2001; Lin et al., 2011). The spatial location of active cells did not vary when we used odors collected from different donor individuals (Figures S1B and S1C) or at different bregma values (Figure S1E).

To more accurately determine the relative location of active ensembles, we concomitantly stained for c-Fos and molecular markers for VMH sub-regions—SF1 for VMH_{dm} and VMH_c, or Esr1 for VMH_{vl} (reviewed in McClellan et al., 2006). In male mice exposed to either cat or snake odors, we observed strong c-Fos and SF1 co-localization (~60%–70%) (Figures 2A and 2B). In contrast, we observed little overlap in animals exposed to odors from another male (Figures 2A and 2B), confirming that this social stimulus does not activate the VMH_{dm}.

Interestingly, the neural ensembles of cat and snake, although SF1⁺, do not seem to grossly overlap in the VMH (Figures 1J and 2A), with the snake-activated cells located in the VMH_c. Additionally, we confirmed that the centrally located snake cells do not overlap with the VMH_{vl} via co-staining with Esr1 (Figures 2B and 2C).

To further corroborate that cat and snake are represented by distinct VMH ensembles, we sequentially exposed mice to one and the other stimulus, followed by dual c-Fos immunostaining

and *in situ* hybridization to locate the nuclear c-Fos protein (indicative of cells activated by snake odor) and the immature nuclear c-Fos mRNA (indicative of stimulation by cat odor) (Figure 2D; exposure controls in Figure S1F–S1H) (Carvalho et al., 2015). This approach confirms that cat and snake ensembles, although both SF1⁺ (Figure 2A), are spatially disjunct (Figure 2D). The overlap level between the two ensembles is very low and not significantly greater than that expected by random activation of VMH cells (3.9% ± 0.9% of all cells expressing c-Fos protein that also express c-Fos mRNA versus 2.1% ± 0.6% overlap expected by chance alone; means ± SEM; Welch's t test assuming unequal variances; t = 0.79; p = 0.24; see STAR Methods for details). The overlap level between the snake and cat ensembles is much less than the overlap seen after two instances of stimulation with snake odor (Figure S1H) (23.4% ± 0.9%, statistically higher than 2.5% ± 0.6% overlap expected by chance [t = 24.3; degrees of freedom {df} = 6; p < 10⁻⁷]). Finally, we probed the relative VMH ensemble locations for snake and male mouse stimuli, confirming that the snake-responsive VMH_c and the conspecific-responsive VMH_{vl} subpopulations are non-overlapping (Figure S1I).

Together, our data show that distinct odors are represented by spatially segregated active VMH ensembles. Interestingly, we found that neurons expressing the same molecular marker (SF1, for example) can be subdivided into distinct cellular types activated by different stimuli. Importantly, our data expose that chemosignal-inducing behaviors within the same general broad categories, such as defensive behavior-triggering cat and snake odors, do not necessarily map onto similarly spatially located ensembles, pointing to the need for deeper understanding of how VMH activity is organized.

The VMH Map Is Dependent on Olfactory Information from the VNO

To dissect the logic behind the organization of VMH activity, we sought to define critical functional inputs to the active ensembles. The VNO has been shown to detect the chemosignals tested in our study (Carvalho et al., 2015; Isogai et al., 2011) and to indirectly connect with the VMH (Blanchard et al., 2005; von Campenhausen and Mori, 2000; Canteras et al., 1995, 1997; Petrovich et al., 2001). We thus hypothesized that the active VMH ensembles depend on VNO sensory information.

Our results show that VNO and VMH activity are closely correlated (stimuli that activate more cells in the VNO also activate more cells in the VMH) (Figures S2A and S2B). Thus, we decided to analyze VMH activity in *TrpC2*^{-/-} mutant animals, which

Figure 1. Olfactory Stimuli Activate Dispersed but Spatially Circumscribed VMH Ensembles

(A–H) Representative images of neural ensembles activated by a range of different stimuli (c-Fos; green), including some located in VMH_{dm} (A–C), VMH_c (D–G), and VMH_{vl} (H). The VMH is outlined by a dashed line. Bregma: -1.46 mm (see also Figure S1E). DAPI staining in purple. Scale bar: 100 μm. d, dorsal; m, medial; 3V, third ventricle; ♂exp♂, male mice exposed to male odors.

(I) c-Fos⁺ cells in subjects exposed to different stimuli. Gray dots represent individual mice. Means + SEM, n = 12–23. unscnt., unscented control; lpd cat, leopard cat. (J) For each stimulus, oval represents distribution of c-Fos⁺ cells pooled from six animals (see STAR Methods for details). The dorsomedial-ventrolateral axis is shown above each oval. Box-whisker plots indicate IQ range of active ensemble distribution along both VMH axes. Bar graphs: c-Fos⁺ cells (means + SEM) along five 100-μm VMH subdivisions. n = 6 mice. See also Figure S1A.

(K) Summary of activated VMH ensemble locations in VMH_{dm}, VMH_c, and VMH_{vl}.

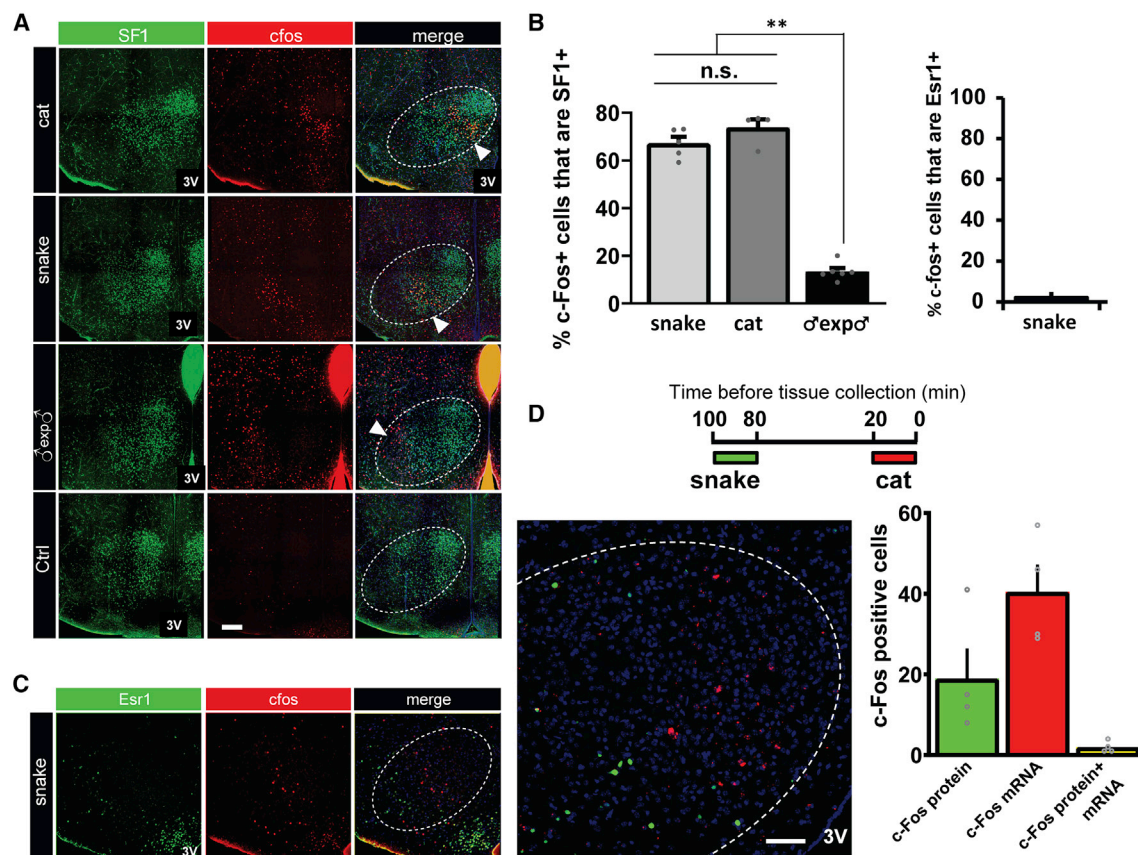


Figure 2. Distinct Odors Activate Non-overlapping Populations of VMH Neurons

(A) Co-staining of VMH sections from cat- and snake-exposed mice for c-Fos (red) and SF1 (green). Ctrl, no stimulation control.

(B) Quantification of SF1 and c-Fos (left) or Esr1 and c-Fos (right) staining overlaps. n.s., non-significant; **p < 0.001. ANOVA followed by honestly significant difference (HSD) post hoc test.

(C) Co-staining of sections from snake-exposed mice for c-Fos (red) and Esr1 (green).

(D) Top: exposure protocol for dual staining experiment (immunostaining for c-Fos protein in green and *in situ* hybridization signal for c-Fos mRNA in red). Bottom: activated VMH cells after sequential exposure to snake and cat stimuli (maximum intensity projection from 30- μ m z series; see related controls in Figures S1F–S1H). Graph shows distribution of activated ensembles labeled for snake stimulus only (green), for cat stimulus only (red), and for both (yellow). Each dot represents one animal. Means + SEM, n = 4 animals. Bregma –1.46 mm. DAPI staining in blue. Scale bars: 100 μ m. 3V, third ventricle.

harbor an inactive VNO (Liman et al., 1999) and display impaired VNO-mediated behaviors (Figure S2C) (Carvalho et al., 2015; Chamero et al., 2007; Kimchi et al., 2007; Papes et al., 2010; Stowers et al., 2002). VMH activation by conspecific and heterospecific odors is abolished in *TrpC2*^{-/-} animals (Figures 3A and 3B). Importantly, *TrpC2*^{-/-} animals normally investigate the sources of odor (Figure S2D) (Papes et al., 2010), and the main olfactory bulb (Figure S2E) and piriform cortex (Carvalho et al., 2015) are still active in these animals, indicating that the loss in VMH activity is not due to lower stimulus sampling. We also observed that pure behavior-inducing stimuli, such as recombinant conspecific and heterospecific major urinary proteins (Chamero et al., 2007; Papes et al., 2010), activate discretely positioned ensembles in the VMH, in a manner that depends on VNO functional input (Figures S3A–S3C).

Taken together, these data indicate that the observed active VMH ensembles are dependent on detection of chemosignals by the VNO.

Stimuli Detected by Different Combinations of VNO Receptors Activate Spatially Disjunct VMH Ensembles

We next sought to determine the principles governing the spatial representation of odors in the VMH. Because VMH activity depends on VNO function (Figures 3A and 3B), it is possible that vomeronasal sensory information defines the location of active VMH neurons. One aspect of sensory information coming from the VNO is the set of vomeronasal receptors expressed in activated neurons. Most stimuli employed in this study are detected by the basal VNO zone (Carvalho et al., 2015; Isogai et al., 2011; this article), whose neurons express V2R vomeronasal receptors (Herrada and Dulac, 1997). V2Rs constitute a family of ~120 members phylogenetically separated into several clades (Figure 3C) (Silvotti et al., 2007).

To test whether the spatial position of VMH ensembles is correlated with the receptors in activated VNO cells, we initially performed double *in situ* hybridization to simultaneously detect the immediate early gene *Egr1* and selected V2R clades

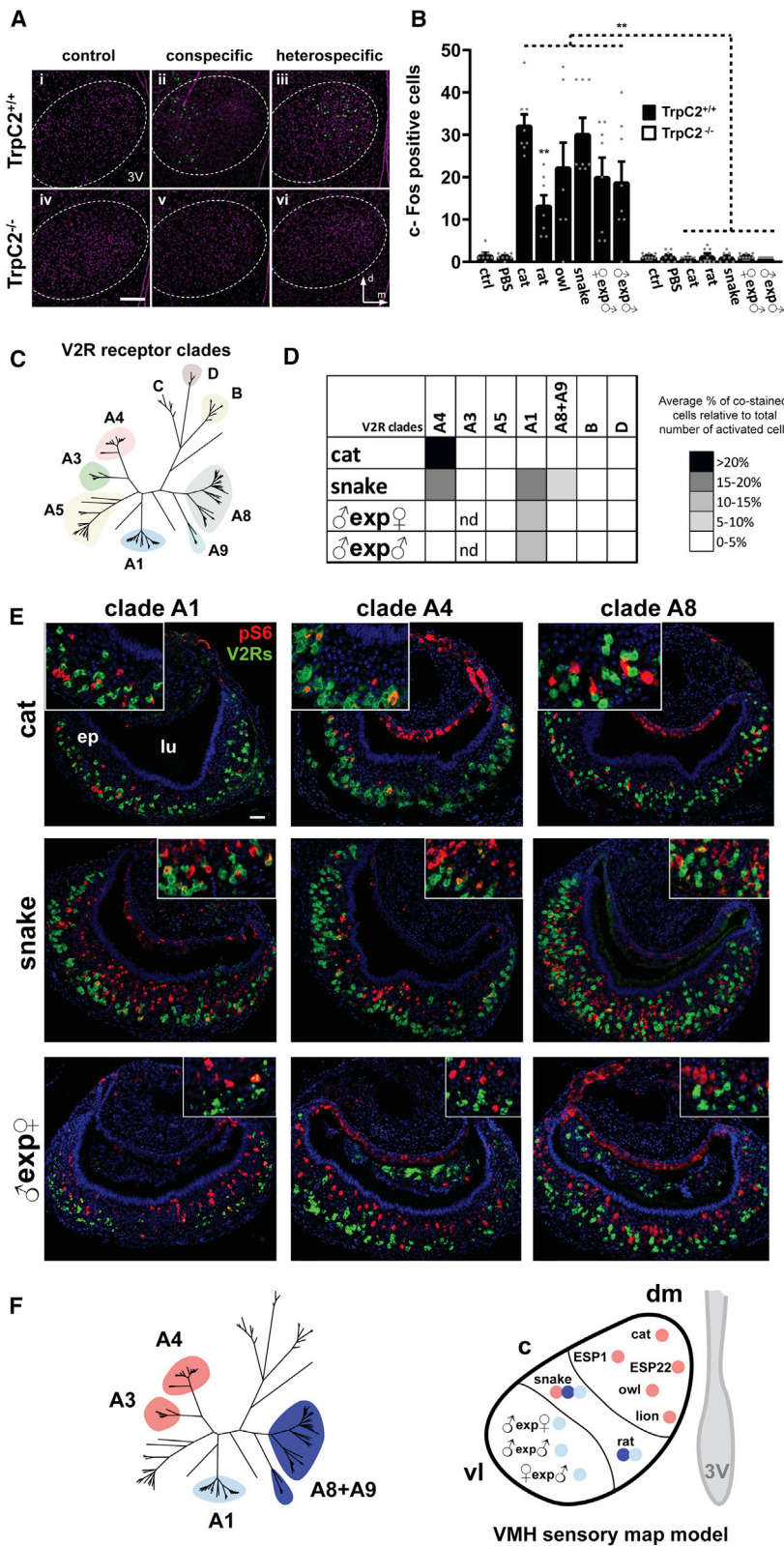


Figure 3. VMH Ensembles Depend on VNO Sensory Input

(A) VMH activation is impaired in *TrpC2*^{-/-} animals. Nuclear staining is in purple.

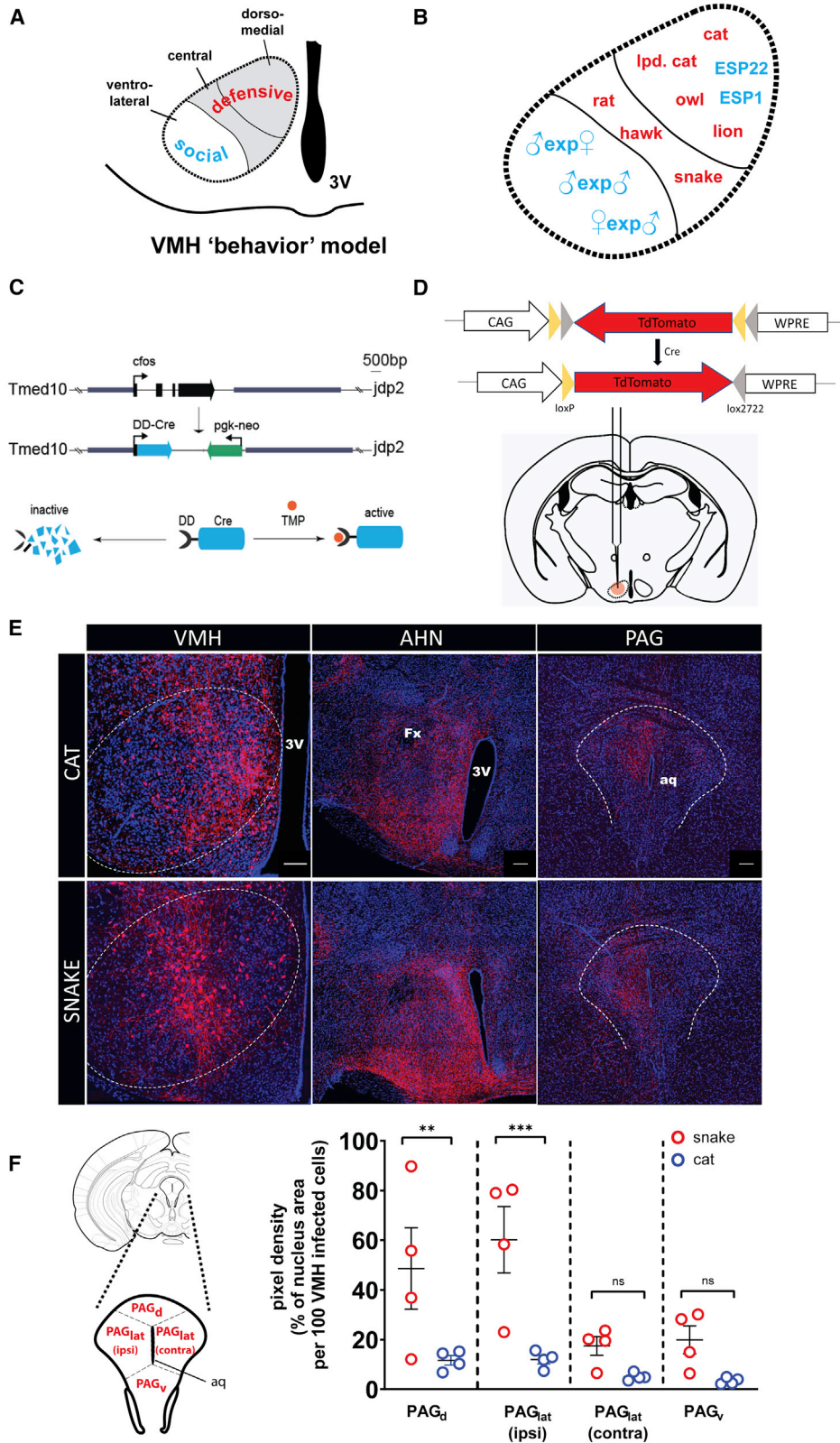
(B) c-Fos quantification in the VMH of *TrpC2*^{+/+} (black bars) and *TrpC2*^{-/-} (white bars) mice. ctrl, control odor (see Table S1). Means + SEM, n = 8 mice. **p < 0.001. ANOVA followed by Tukey-Kramer HSD post hoc analysis (comparison of *TrpC2*^{+/+} against *TrpC2*^{-/-} for each odor).

(C) V2R receptor phylogenetic tree (clade nomenclature as in Silvotti et al. [2007]).

(D) Heatmap of V2R receptors in activated VNO neurons for various stimuli (quantification in Table S2). Figure S4 and Isogai et al. (2011) show other clades and stimuli.

(E) Co-localization of V2R receptors (green) and pS6 (red) in the VNO of mice exposed to various stimuli (high-magnification images in insets). See also Figure S4A. Nuclear staining in blue.

(F) Location of active VMH ensembles for stimuli detected by V2R receptors in clades A4 and A3 (orange dots), A1 (light blue), and A8 (dark blue). d, dorsal; m, medial; 3V, third ventricle; lu, lumen; ep, sensory epithelium. Scale bar: 100 μm.



(legend on next page)

(Figure S4B) (as described in Isogai et al. [2011]). During the course of our study, phosphorylated ribosomal protein S6 (pS6) became available as a better marker for olfactory neuron activation (Jiang et al., 2015; Knight et al., 2012). We then combined *in situ* hybridization for V2R clades with pS6 immunostaining (see Carvalho et al. [2015] for probe design and validation).

Cat odors, which activate the VMH_{dm}, are mainly detected by VNO cells expressing clade A4 V2R receptors (Figures 3D, 3E, and S4A; Table S2; see also Figure S4B for *Egr1* staining). Pheromone ESP22 (exocrine gland-secreting peptide 22), which also induces activity in the VMH_{dm} (Figures 3F and S3D) (Osakada et al., 2018), is detected by a receptor in clade A3 (Ferrero et al., 2013), closely related to A4.

On the other hand, snake odors are detected by a combination of A1, A4, and A8 V2R receptors (Figures 3D–3F and S4A) and induce neural activity in SF1⁺ VMH_c (Figure 1J). Rat odors also result in an active ensemble in the VMH_c (Figures 1J and S3C) and are detected by a similar combination of A4 and A8 V2R receptors (Figures 3D–3F and S4C; see also Isogai et al. [2011]).

Finally, male and female mouse odors, which activate a VMH_{vl} ensemble in male mice (Figures 1H, 1J, 1K, and S1D), are detected mostly by A1 receptors (Figures 3D–3F and S4A; Table S2).

These results suggest that the identity of activated VNO receptors influence the spatial location of active VMH ensembles. At this level of coarse resolution, activation of receptors in A3/A4 clades is associated with active ensembles in the VMH_{dm}, whereas combinations of A1 + A4 + A8 or A4 + A8 V2R receptors shift the representation toward the VMH_c, and activation of A1 receptors is linked to VMH_{vl} activity (Figure 3F).

Defensive and Social Chemosignals Can Activate Similarly Positioned VMH Ensembles

The VMH has long been proposed to be divided into social and defensive sectors (Figure 4A) (Choi et al., 2005; Dielenberg et al., 2001; Lin et al., 2011; Silva et al., 2013; Swanson, 2000). However, our results imply that odors that elicit behavioral responses belonging to the same category do not necessarily activate similarly positioned spatial VMH ensembles (Figure 4B). For instance, cat and snake odors both induce defensive fear-like behaviors (Figure S2C) (Dielenberg et al., 2001; Papes et al., 2010), yet they activate cells that are differently positioned and mostly non-overlapping in the VMH_{dm} and VMH_c, respectively (Figures 1J and 4B), exposing the existence of further subdivisions within the so-called “defensive zone.”

Moreover, the conspecific stimulus ESP22 peptide elicits activity in the VMH_{dm} (Figure S3D) (Osakada et al., 2018). This juvenile-derived pheromone modulates social behavior (inhibition of

adult sexual behavior) (Ferrero et al., 2013) but maps onto the same VMH sector activated by defensive behavior-inducing cat odor stimulus (Figures 1J and 4B).

Finally, our data show that stimuli that alter male social (sexual) behaviors—ESP22 and female odors—activate dissimilarly positioned ensembles in the VMH_{dm} and VMH_{vl}, respectively (Figures 1J, 4B, and S3D). Likewise, in females, male odors activate the VMH_{vl} (Figures 1I, 1K, and S3E) and are detected by A1 receptors (Figure 3F) (Isogai et al., 2011), whereas another male chemosignal, ESP1 peptide, activates the VMH_{dm} (Ishii et al., 2017) and is detected by an A3 receptor (Figure S4C) (Haga et al., 2010).

Together, these data show that the VMH is not organized according to broad behavior categories, indicating the need for a revision of the current dichotomous functional division of the VMH into defensive versus social regions.

Labeling Spatially Disjunct Active VMH Ensembles Reveals Differential Downstream Projection Targets

It remains to be understood how VMH subpopulations activated by distinct odors project in the brain. Cat and snake odors elicit defensive behaviors, yet they are represented in distinct subregions of the VMH (VMH_{dm} and VMH_c, respectively). One possibility is that cat and snake active VMH ensembles exhibit similar projection patterns to downstream effector nuclei because they induce behaviors in the same broad category. Alternatively, they may exhibit differential connections with downstream targets, following the distinct projection patterns previously observed for the VMH_{dm} and VMH_c subregions in which such ensembles lie (Canteras et al., 1994).

We devised a strategy that allowed us to separately label projections from the cat or snake VMH ensembles, using a knockin mouse line (Dillingham et al., 2019), in which Cre fused to a destabilizing domain (DD-Cre) is under the control of the *c-Fos* promoter (FDC mice) (Figure 4C). Injection of FDC mice with an adeno-associated virus (AAV) vector carrying Cre-dependent axon-filling tdTomato (Figure 4D), followed by administration of trimethoprim (TMP), results in stabilized and catalytically active DD-Cre and, therefore, tdTomato labeling of activated neurons.

First, we confirmed that we were able to accurately target the VMH during viral injections (Figure 4E) in animals exposed to either cat or snake stimuli, and the locations of tdTomato⁺ cells were concordant with the presumptive location of the respective active ensembles in VMH_{dm} and VMH_c (Figures 1A, 1F, and 1J).

Next, we chose to analyze two known VMH projection sites, the anterior hypothalamic nucleus (AHN) and the periaqueductal gray (PAG) (Canteras et al., 1994), shown to directly influence different aspects of defensive behavior (Wang et al., 2015).

Figure 4. Comparison between Positions of Active VMH Ensembles and Output Behaviors or Projection Patterns

(A) Current “behavioral” model of VMH organization, with VMH_{dm} and VMH_c involved in defensive behaviors (gray shading) and VMH_{vl} linked to social behaviors. (B) Comparison between position of active ensembles and behaviors for various odors (defensive in red; social in blue). (C) *c-Fos::DD-Cre* (FDC) mouse tracing strategy to label projection sites for VMH ensembles responsive to distinct odors. (D) Viral vector with double-inverted floxed tdTomato gene for Cre-dependent expression of tdTomato in *c-Fos*⁺ neurons. (E) VMH, AHN, and PAG images from viral-transduced FDC mice exposed to cat or snake odors. 3V, third ventricle; Fx, fornix; aq, cerebral aqueduct. Bars are 100 μm (VMH), 150 μm (AHN), or 120 μm (PAG). (F) Normalized tdTomato⁺ fiber density (right); percentage of area occupied by positive fibers in the PAG subdivisions (left). Means ± SEM, n = 4 animals; **p < 0.01, ***p < 0.001; one-way analysis of variance followed by HSD post hoc test. DAPI staining is in blue. aq, cerebral aqueduct.

Both sites were densely innervated with tdTomato⁺ fibers (Figure 4E). At this resolution level, we could not detect any gross differences in the density of labeled AHN fibers between cat- and snake-exposed animals (Figure 4E; 33.38 ± 15.2 normalized pixel density for snake stimulus versus 18.05 ± 1.04 for cat; not statistically significant in Welch's two-tailed t test assuming unequal variances: $t = 0.774$, $p = 0.519$; see STAR Methods for details).

When we analyzed different sectors of the PAG (Figure 4F, left), we observed dense ipsi-lateral innervation in the dorsal and lateral PAG (PAG_d and PAG_{lat}, respectively), whereas the contra-lateral side was only marginally occupied by tdTomato⁺ fibers (Figures 4E and 4F). Interestingly, when the density of fibers (percentage of the nucleus area occupied by tdTomato⁺ pixels) was normalized against the number of AAV-infected cell bodies in the VMH, the snake stimulus showed heavier innervation in both PAG_d and PAG_{lat} (ipsi) than the cat stimulus did (Figure 4F). Moreover, linear-fit regression analysis between tdTomato⁺ cell bodies in the VMH and the pixel density in the PAG_d and PAG_v showed that an increase in labeled VMH cells is correlated with a more pronounced fiber-density increase in PAG_d than it is in the PAG_v (Figure S4D). This effect is much less evident for cat stimulus, suggesting a preferential input from the snake-responsive cells in VMH_c to the PAG_d when compared with the cat-responsive cells in VMH_{dm}.

We used viral constructs that were not designed to restrict tdTomato expression to the VMH, and we observed tdTomato⁺ cell bodies in neighboring nuclei, such as the dorsomedial nucleus of the hypothalamus (DMH) and the lateral hypothalamic area (LHA). However, the number of labeled cell bodies is much higher in the VMH than in the DMH or LHA (Figure S4E). Moreover, DMH staining was absent in two animals, yet they still exhibited PAG labeling (Figure S4E), and the DMH-PAG correlation was less significant than the VMH-PAG correlation was (*R*-squared coefficients: 0.36 [DMH] versus 0.86 [VMH], for snake stimulus). Although confirmatory experiments are needed with methods that allow the VMH to be specifically labeled, these controls suggest that the contribution from stained VMH cell bodies to PAG projections is more evident than it is from stained cells in neighboring nuclei.

Together, our tracing data suggest that VMH ensembles responsive to different odors send differential projections to distinct sub-regions of the PAG.

DISCUSSION

In this study, we investigated the neural mapping of behavior-inducing odors in the hypothalamus. We show that distinct odors entail a variety of spatial patterns of activity in the VMH (Figure 1) and that these active ensembles depend on VNO sensory information (Figure 3). Each stimulus stereotypically activates a population of VMH neurons in a defined spatial location (Figure 1). This is similar to the organization of pheromone information in the lateral horn of the fly (Fisek and Wilson, 2014) and of taste information in the mammalian brain (Chen et al., 2011) but contrasts with the non-stereotypical, dispersed representation of odorants in the piriform cortex (Ghosh et al., 2011; Miyamichi et al., 2011; Schaffer et al., 2018; Sosulski et al., 2011).

Our observations show that stimuli detected by different combinations of vomeronasal receptors induce activity in spatially segregated VMH ensembles (Figure 3). These results suggest the interesting possibility that the activated set of vomeronasal receptors for each stimulus dictates the corresponding pattern of VMH activity, forming a sensory neural map. Because most odors employed in our assays activate the basal layer of the VNO, we focused our analysis on the V2R vomeronasal receptor family. It will be interesting to understand how stimuli detected by V1R and FPR vomeronasal receptors (reviewed in Munger et al. [2009]) are represented in the VMH.

The correlation between activated receptor repertoires and the active VMH ensembles will need to be further characterized with finer resolution, for example, via Act-Seq single-cell RNA sequencing (RNA-seq). It should be noted, however, that immediate early genes do not capture all details of activity-response profile dynamics and that differences in crude stimulus strength or subject investigation may affect sensory detection. Moreover, VNO activation is changed by biological context and internal hormonal state (Dey et al., 2015), such that the neural representation of sensory information might include additional layers of complexity, which our 2D mapping did not probe. Despite these caveats, fiber photometry and micro-endoscopy experiments strongly suggest that stimulus identity is preserved in the VMH (Kennedy et al., 2019), supporting the sensory map proposed here.

In principle, this sensory model of VMH organization is not mutually exclusive with the possibility that the nucleus is divided according to the behavioral consequences of each detected stimulus. However, our data challenge the currently accepted theory that the VMH is dichotomously divided into defensive and social functional sectors (Figure 4A) (Choi et al., 2005; Swanson, 2000) because similarly positioned VMH ensembles for some stimuli are correlated with different behaviors (Figure 4B). In agreement with this assessment, a recent publication found that each sub-population of VMH cells may be correlated with more than one behavior category, whereas different subpopulations can be related to the same behavior category (Kim et al., 2019).

An interesting counterpoint is that certain olfactory stimuli that apparently induce behaviors in different broad categories may map onto the same location in the VMH because they operate to modulate a common behavioral aspect. For example, ESP22 and predator odors are social and defensive stimuli, respectively (Ferrero et al., 2013; Osakada et al., 2018; Papes et al., 2010), but both inhibit social interaction, which could justify their similarly positioned VMH ensembles. Another pondering is that our behavioral assays were not devised to capture nuances in behavioral output; therefore, behaviors in the same general category (e.g., cat- and snake-induced defensive behaviors) may be slightly but sufficiently distinct to justify differently positioned active VMH ensembles.

The results presented here indicate that cat- and snake-responsive VMH subpopulations are not similarly connected to downstream targets (Figures 4C–4F). The VMH_{dm} and VMH_c sectors in which those ensembles are located have been previously shown to project differentially in the brain (Canteras et al., 1994). In the future, it will be interesting to verify whether the snake and cat ensembles follow the published projection

patterns for the VMH_{dm} and VMH_c, or if they exhibit differential projections beyond what would be expected based on their sites of origin.

Altogether, it is interesting that olfactory information is internally represented so far removed from the olfactory organs. The accessory olfactory bulb, the first relay station after the VNO, preserves information about stimulus identity because VNO neurons expressing distinct receptors are connected with different groups of bulb glomeruli (Wagner et al., 2006). In the medial nucleus of the amygdala (MeA), downstream to the bulb and upstream to the VMH, distinct stimuli activate spatially intermingled subpopulations of cells, some of which respond to specific chemosignals (Bergan et al., 2014; Carvalho et al., 2015). Therefore, it is possible that sensory information is maintained up until the VMH, although further work is required to understand how each type of neural map transitions to the next station.

STAR★METHODS

Detailed methods are provided in the online version of this paper and include the following:

- KEY RESOURCES TABLE
- RESOURCE AVAILABILITY
 - Lead Contact
 - Materials Availability
 - Data and Code Availability
- EXPERIMENTAL MODEL AND SUBJECT DETAILS
 - Animals
- METHOD DETAILS
 - Olfactory stimuli
 - Expression of recombinant Mup and ESP stimuli
 - Behavioral assays
 - Immunostaining procedures
 - *In situ* hybridization and dual staining
 - Viral tracing in FDC mice
- QUANTIFICATION AND STATISTICAL ANALYSIS

SUPPLEMENTAL INFORMATION

Supplemental Information can be found online at <https://doi.org/10.1016/j.celrep.2020.108061>.

ACKNOWLEDGMENTS

We thank G.A.G. Pereira, J.A. Yunes, and P. Cameron for sharing resources; A.R. Castro, G.L. Castro, and D.M. Mendes for providing snake and spider odors; N.D.M. Villanueva for help with statistical analyses; M.L. Justino for help with artwork; the Life Sciences Core Facility (LaCTAD-UNICAMP) staff and K. Spencer (Scripps Research) for help with confocal microscopy; Dr. M. Mayford for providing AAV vector; and Dr. S. Liberles for providing ESP expression constructs. This work was supported by the São Paulo Research Foundation (FAPESP; grant numbers 2009/00473-0 and 2015/50371-0 to F.P.); by PRP/UNICAMP (grant numbers 2969/16, 725/15, 348/14, and 315/12 to F.P.); by FAPESP fellowships to V.M.A.C. (2014/25594-3, 2012/21786-0, and 2012/01689-0), to T.S.N. (2012/04026-1), to M.A.A.S. (2013/03372-6), and to L.M.C. (2010/01211-7); and by a Coordenação de Aperfeiçoamento de Pessoal de Nível Superior (CAPES) fellowship to T.S.N.

AUTHOR CONTRIBUTIONS

Conceptualization, V.M.A.C., L.S., and F.P.; Methodology, V.M.A.C., T.S.N., and F.P.; Investigation, V.M.A.C., T.S.N., M.A.A.S., L.M.C., G.Z.T., L.G.P., J.O.V.; Writing – Original Draft, V.M.A.C., and F.P.; Writing – Review & Editing, V.M.A.C., and F.P.; Funding Acquisition, V.M.A.C., and F.P.; Resources, L.S., and F.P.; Supervision, F.P.

DECLARATION OF INTERESTS

The authors declare no competing interests.

Received: January 23, 2020

Revised: May 20, 2020

Accepted: July 31, 2020

Published: August 25, 2020

REFERENCES

- Bergan, J.F., Ben-Shaul, Y., and Dulac, C. (2014). Sex-specific processing of social cues in the medial amygdala. *eLife* 3, e02743.
- Blanchard, D.C., Canteras, N.S., Markham, C.M., Pentkowski, N.S., and Blanchard, R.J. (2005). Lesions of structures showing FOS expression to cat presentation: effects on responsivity to a Cat, Cat odor, and nonpredator threat. *Neurosci. Biobehav. Rev.* 29, 1243–1253.
- Canteras, N.S., Simerly, R.B., and Swanson, L.W. (1994). Organization of projections from the ventromedial nucleus of the hypothalamus: a Phaseolus vulgaris-leucoagglutinin study in the rat. *J. Comp. Neurol.* 348, 41–79.
- Canteras, N.S., Simerly, R.B., and Swanson, L.W. (1995). Organization of projections from the medial nucleus of the amygdala: a PHAL study in the rat. *J. Comp. Neurol.* 360, 213–245.
- Canteras, N.S., Chiavegatto, S., Ribeiro do Valle, L.E., and Swanson, L.W. (1997). Severe reduction of rat defensive behavior to a predator by discrete hypothalamic chemical lesions. *Brain Res. Bull.* 44, 297–305.
- Carvalho, V.M., Nakahara, T.S., Cardozo, L.M., Souza, M.A., Camargo, A.P.C.B.R., Trintinalia, G.Z., Ferraz, E., and Papes, F. (2015). Lack of spatial segregation in the representation of pheromones and kairomones in the mouse medial amygdala. *Front. Neurosci.* 9, 283.
- Chamero, P., Marton, T.F., Logan, D.W., Flanagan, K., Cruz, J.R., Saghatelian, A., Cravatt, B.F., and Stowers, L. (2007). Identification of protein pheromones that promote aggressive behaviour. *Nature* 450, 899–902.
- Chen, X., Gabitto, M., Peng, Y., Ryba, N.J.P., and Zuker, C.S. (2011). A gustotopic map of taste qualities in the mammalian brain. *Science* 333, 1262–1266.
- Choi, G.B., Dong, H.W., Murphy, A.J., Valenzuela, D.M., Yancopoulos, G.D., Swanson, L.W., and Anderson, D.J. (2005). Lhx6 delineates a pathway mediating innate reproductive behaviors from the amygdala to the hypothalamus. *Neuron* 46, 647–660.
- Dey, S., Chamero, P., Pru, J.K.K., Chien, M.-S., Ibarra-Soria, X., Spencer, K.R.R., Logan, D.W.W., Matsunami, H., Peluso, J.J.J., and Stowers, L. (2015). Cyclic regulation of sensory perception by a female hormone alters behavior. *Cell* 161, 1334–1344.
- Dielenberg, R.A., Hunt, G.E., and McGregor, I.S. (2001). “When a rat smells a cat”: the distribution of Fos immunoreactivity in rat brain following exposure to a predatory odor. *Neuroscience* 104, 1085–1097.
- Dillingham, B.C., Cameron, P., Pieraut, S., Cardozo, L.M., Yoo, E.J., Maximov, A., Stowers, L., and Mayford, M. (2019). Fear learning induces long-lasting changes in gene expression and pathway specific presynaptic growth. *bioRxiv*. <https://doi.org/10.1101/571331>.
- Ferrero, D.M., Moeller, L.M., Osakada, T., Horio, N., Li, Q., Roy, D.S., Cichy, A., Spehr, M., Touhara, K., and Liberles, S.D. (2013). A juvenile mouse pheromone inhibits sexual behaviour through the vomeronasal system. *Nature* 502, 368–371.
- Fişek, M., and Wilson, R.I. (2014). Stereotyped connectivity and computations in higher-order olfactory neurons. *Nat. Neurosci.* 17, 280–288.

- Ghosh, S., Larson, S.D., Hefzi, H., Marnoy, Z., Cutforth, T., Dokka, K., and Baldwin, K.K. (2011). Sensory maps in the olfactory cortex defined by long-range viral tracing of single neurons. *Nature* *472*, 217–220.
- Guzowski, J.F., McNaughton, B.L., Barnes, C.A., and Worley, P.F. (1999). Environment-specific expression of the immediate-early gene *Arc* in hippocampal neuronal ensembles. *Nat. Neurosci.* *2*, 1120–1124.
- Guzowski, J.F., McNaughton, B.L., Barnes, C.A., and Worley, P.F. (2001). Imaging neural activity with temporal and cellular resolution using FISH. *Curr. Opin. Neurobiol.* *11*, 579–584.
- Haga, S., Hattori, T., Sato, T., Sato, K., Matsuda, S., Kobayakawa, R., Sakano, H., Yoshihara, Y., Kikusui, T., and Touhara, K. (2010). The male mouse pheromone ESP1 enhances female sexual receptive behaviour through a specific vomeronasal receptor. *Nature* *466*, 118–122.
- Hashikawa, K., Hashikawa, Y., Tremblay, R., Zhang, J., Feng, J.E., Sabol, A., Piper, W.T., Lee, H., Rudy, B., and Lin, D. (2017). *Esr1*⁺ cells in the ventromedial hypothalamus control female aggression. *Nat. Neurosci.* *20*, 1580–1590.
- Herrada, G., and Dulac, C. (1997). A novel family of putative pheromone receptors in mammals with a topographically organized and sexually dimorphic distribution. *Cell* *90*, 763–773.
- Ishii, K.K., Osakada, T., Mori, H., Miyasaka, N., Yoshihara, Y., Miyamichi, K., and Touhara, K. (2017). A Labeled-line neural circuit for pheromone-mediated sexual behaviors in mice. *Neuron* *95*, 123–137.e8.
- Isogai, Y., Si, S., Pont-Lezica, L., Tan, T., Kapoor, V., Murthy, V.N., and Dulac, C. (2011). Molecular organization of vomeronasal chemoreception. *Nature* *478*, 241–245.
- Iwamoto, M., Björklund, T., Lundberg, C., Kirik, D., and Wandless, T.J. (2010). A general chemical method to regulate protein stability in the mammalian central nervous system. *Chem. Biol.* *17*, 981–988.
- Jiang, Y., Gong, N.N., Hu, X.S., Ni, M.J., Pasi, R., and Matsunami, H. (2015). Molecular profiling of activated olfactory neurons identifies odorant receptors for odors in vivo. *Nat. Neurosci.* *18*, 1446–1454.
- Kennedy, A., Kunwar, P.S., Li, L., Wagenaar, D., and Anderson, D.J. (2019). Stimulus-specific neural encoding of a persistent, internal defensive state in the hypothalamus. *bioRxiv*. <https://doi.org/10.1101/805317>.
- Kim, D.-W., Yao, Z., Grayback, L.T., Kim, T.K., Nguyen, T.N., Smith, K.A., Fong, O., Yi, L., Kouloua, N., Pierson, N., et al. (2019). Multimodal analysis of cell types in a hypothalamic node controlling social behavior. *Cell* *179*, 713–728.e17.
- Kimchi, T., Xu, J., and Dulac, C. (2007). A functional circuit underlying male sexual behaviour in the female mouse brain. *Nature* *448*, 1009–1014.
- Knight, Z.A., Tan, K., Birsoy, K., Schmidt, S., Garrison, J.L., Wysocki, R.W., Emiliano, A., Ekstrand, M.I., and Friedman, J.M. (2012). Molecular profiling of activated neurons by phosphorylated ribosome capture. *Cell* *151*, 1126–1137.
- Kunwar, P.S., Zelikowsky, M., Remedios, R., Cai, H., Yilmaz, M., Meister, M., and Anderson, D.J. (2015). Ventromedial hypothalamic neurons control a defensive emotion state. *eLife* *4*, e06633.
- Lee, H., Kim, D.-W., Remedios, R., Anthony, T.E., Chang, A., Madisen, L., Zeng, H., and Anderson, D.J. (2014). Scalable control of mounting and attack by *Esr1*⁺ neurons in the ventromedial hypothalamus. *Nature* *509*, 627–632.
- Liman, E.R., Corey, D.P., and Dulac, C. (1999). TRP2: a candidate transduction channel for mammalian pheromone sensory signaling. *Proc. Natl. Acad. Sci. USA* *96*, 5791–5796.
- Lin, D., Boyle, M.P., Dollar, P., Lee, H., Lein, E.S., Perona, P., and Anderson, D.J. (2011). Functional identification of an aggression locus in the mouse hypothalamus. *Nature* *470*, 221–226.
- Lo, L., Yao, S., Kim, D.W., Cetin, A., Harris, J., Zeng, H., Anderson, D.J., and Weissbourd, B. (2019). Connective architecture of a mouse hypothalamic circuit node controlling social behavior. *Proc. Natl. Acad. Sci. USA* *116*, 7503–7512.
- Logan, D.W., Marton, T.F., and Stowers, L. (2008). Species specificity in major urinary proteins by parallel evolution. *PLoS ONE* *3*, e3280.
- McClellan, K.M., Parker, K.L., and Tobet, S. (2006). Development of the ventromedial nucleus of the hypothalamus. *Front. Neuroendocrinol.* *27*, 193–209.
- Miyamichi, K., Amat, F., Moussavi, F., Wang, C., Wickersham, I., Wall, N.R., Taniguchi, H., Tasic, B., Huang, Z.J., He, Z., et al. (2011). Cortical representations of olfactory input by trans-synaptic tracing. *Nature* *472*, 191–196.
- Munger, S.D., Leinders-Zufall, T., and Zufall, F. (2009). Subsystem organization of the mammalian sense of smell. *Annu. Rev. Physiol.* *71*, 115–140.
- Osakada, T., Ishii, K.K., Mori, H., Eguchi, R., Ferrero, D.M., Yoshihara, Y., Liberles, S.D., Miyamichi, K., and Touhara, K. (2018). Sexual rejection via a vomeronasal receptor-triggered limbic circuit. *Nat. Commun.* *9*, 4463.
- Papes, F., Logan, D.W., and Stowers, L. (2010). The vomeronasal organ mediates interspecies defensive behaviors through detection of protein pheromone homologs. *Cell* *141*, 692–703.
- Papes, F., Nakahara, T.S., and Camargo, A.P. (2018). Behavioral assays in the study of olfaction: a practical guide. *Methods Mol Biol.* *1820*, 289–388.
- Petrovich, G.D., Canteras, N.S., and Swanson, L.W. (2001). Combinatorial amygdalar inputs to hippocampal domains and hypothalamic behavior systems. *Brain Res. Brain Res. Rev.* *38*, 247–289.
- Remedios, R., Kennedy, A., Zelikowsky, M., Grewe, B.F., Schnitzer, M.J., and Anderson, D.J. (2017). Social behaviour shapes hypothalamic neural ensemble representations of conspecific sex. *Nature* *550*, 388–392.
- Sando, R., 3rd, Baumgaertel, K., Pieraut, S., Torabi-Rander, N., Wandless, T.J., Mayford, M., and Maximov, A. (2013). Inducible control of gene expression with destabilized Cre. *Nat. Methods* *10*, 1085–1088.
- Schaffer, E.S., Stettler, D.D., Kato, D., Choi, G.B., Axel, R., and Abbott, L.F. (2018). Odor perception on the two sides of the brain: consistency despite randomness. *Neuron* *98*, 736–742.e3.
- Silva, B.A., Mattucci, C., Krzywkowski, P., Murana, E., Illarionova, A., Grinevich, V., Canteras, N.S., Ragozzino, D., and Gross, C.T. (2013). Independent hypothalamic circuits for social and predator fear. *Nat. Neurosci.* *16*, 1731–1733.
- Silvotti, L., Moiani, A., Gatti, R., and Tirindelli, R. (2007). Combinatorial co-expression of pheromone receptors, V2Rs. *J. Neurochem.* *103*, 1753–1763.
- Sosulski, D.L., Bloom, M.L., Cutforth, T., Axel, R., and Datta, S.R. (2011). Distinct representations of olfactory information in different cortical centres. *Nature* *472*, 213–216.
- Stowers, L., Holy, T.E., Meister, M., Dulac, C., and Koentges, G. (2002). Loss of sex discrimination and male-male aggression in mice deficient for TRP2. *Science* *295*, 1493–1500.
- Swanson, L.W. (2000). Cerebral hemisphere regulation of motivated behavior. *Brain Res.* *886*, 113–164.
- Tai, K., Quintino, L., Isaksson, C., Gussing, F., and Lundberg, C. (2012). Destabilizing domains mediate reversible transgene expression in the brain. *PLoS ONE* *7*, e46269.
- von Campenhausen, H., and Mori, K. (2000). Convergence of segregated pheromonal pathways from the accessory olfactory bulb to the cortex in the mouse. *Eur. J. Neurosci.* *12*, 33–46.
- Wagner, S., Gresser, A.L., Torello, A.T., and Dulac, C. (2006). A multireceptor genetic approach uncovers an ordered integration of VNO sensory inputs in the accessory olfactory bulb. *Neuron* *50*, 697–709.
- Wang, L., Chen, I.Z., and Lin, D. (2015). Collateral pathways from the ventromedial hypothalamus mediate defensive behaviors. *Neuron* *85*, 1344–1358.

STAR★METHODS

KEY RESOURCES TABLE

REAGENT or RESOURCE	SOURCE	IDENTIFIER
Antibodies		
Rabbit polyclonal anti-c-Fos	Millipore	Cat# Ab5; RRID:AB_2314043
Rabbit polyclonal anti-c-Fos	Santa-Cruz	Cat# sc-52; RRID:AB_2106783
Goat polyclonal anti-c-Fos	Santa-Cruz	Cat# sc-52 g; RRID:AB_2629503
Rabbit polyclonal anti-ER α	Santa-Cruz	Cat# sc-542; RRID:AB_631470
Rabbit polyclonal anti-SF1	TransGenic	Cat# KO611; RRID:AB_2861370
Rabbit polyclonal anti-pS6	Thermo Scientific	Cat# 44-923G; RRID:AB_1502034
Rabbit polyclonal anti-dinitrophenyl (DNP)	Molecular Probes (Thermo)	Cat# A6430; RRID:AB_221552
Rabbit polyclonal anti-digoxigenin (DIG), conjugated with horseradish peroxidase	Roche (Merck)	Cat# 11207733910, RRID:AB_514500
Bacterial and Virus Strains		
AAV1.CAG.flex.TdTomato.WPRE.rBG	Kindly provided by Mark Mayford's lab (UCSD)	N/A
Chemicals, Peptides, and Recombinant Proteins		
Recombinant cat Mup (Fel-d-4) construct	Papes et al., 2010	N/A
Recombinant rat Mup (Mup13) construct	Logan et al., 2008	N/A
Recombinant mouse Mup constructs	Papes et al., 2010	N/A
Recombinant ESP peptide constructs	Kindly provided by Stephen Liberles' lab	N/A
Critical Commercial Assays		
TSA Biotin System	Perkin Elmer	Cat# NEL700A001KT
Alexa Fluor 555 Tyramide Superboost	Invitrogen	Cat# B40923
Alexa Fluor 488 Tyramide Superboost	Invitrogen	Cat# B40932
Experimental Models: Organisms/Strains		
Mouse: c-Fos::DD-Cre transgenic (B6.Cg-Tg(Fos-DD-Cre) or FDC mouse line	This paper; Dillingham et al., 2019	N/A
Mouse: TrpC2 ^{-/-} transgenic knockout mouse line (<i>Trpc2^{tm1Dlc}</i>)	Stowers et al., 2002	N/A

RESOURCE AVAILABILITY

Lead Contact

Further information and requests for resources and reagents should be directed to and will be fulfilled by the Lead Contact, Fabio Papes (papesf@unicamp.br).

Materials Availability

All unique reagents generated in this study are available from the Lead Contact with a completed Materials Transfer Agreement.

Data and Code Availability

This study did not generate any unique datasets or code.

EXPERIMENTAL MODEL AND SUBJECT DETAILS

Animals

Animals were C57BL/6, FDC or *TrpC2* eight to twelve-weeks-old male mice. *TrpC2*^{+/+} and *TrpC2*^{-/-} are littermates from heterozygous mating couples in C57BL/6 genetic background ([Papes et al., 2010](#)). Mice were housed 1-5 individuals per cage and husbandry conditions were set to 1 male and 1-2 females per breeding cage. All animals had free access to food and water. Prior to each experiment, mice were individually housed for 4 days. Animal procedures were carried out in accordance with Animal Protocol no. 1883-1,

approved by the University of Campinas - Institute of Biology's Institutional Animal Care and Use Committee (Committee for Ethics in Animal Use in Research). This protocol follows guidelines established by the National Council for Animal Experimentation Control (CONCEA-Brazil). For experimental design, group size was determined by statistical power analysis based on variances observed in the literature and in pilot studies, considering 0.05 significance level for type II error and a target power between 0.8 and 0.9.

METHOD DETAILS

Olfactory stimuli

Table S1 shows the list of stimuli employed in this study, including respective quantities and methods of collection. More details can be found in our previous study (Carvalho et al., 2015). For pure stimuli (recombinant proteins) in Figure S3, we expressed mouse Mups, rat Mup13 (Logan et al., 2008), Fel-d-4 cat Mup (Papes et al., 2010) and ESP22 peptide (Ferrero et al., 2013) as fusion proteins with Maltose Binding Protein, which was used as control stimulus. For all stimuli deposited on gauzes, the gauze was unscented in a desiccator under vacuum overnight before adding the stimulus. For solid or liquid stimuli deposited on gauze, they were attached to 'clips' to prevent the stimuli from moving about the cage and to easily visually confirm their position in the recorded videos.

Crude stimuli certainly vary in terms of stimulus strength, and the amounts used here (Table S1) were determined empirically to provide VMH activation. However, two lines of evidence indicate that different stimulus quantities would not result in distinctly located active spatial ensembles. First, exposure to odors from different cats and snakes (with potentially somewhat differing stimulus strengths) do not result in changes in spatial location of the active ensembles for the same stimulus (Figures S1B and S1C). Second, purified stimuli – cat and rat Mups – are certainly less strong than the corresponding crude stimuli, because they activate fewer cells, but the overall location of the respective ensembles remains unaltered (Figures S3A–S3C).

Expression of recombinant Mup and ESP stimuli

cDNA expression constructs for rat Major Urinary Protein (rat Mup13), mouse Mup24 and Mup25 (Logan et al., 2008), cat Mup (Papes et al., 2010), and ESP22 peptide (Ferrero et al., 2013) were expressed as fusion proteins in vector pMAL-c2x, following previously published purification protocols (Carvalho et al., 2015). Protein was eluted from amylose affinity resin using maltose and then equilibrated in 1x PBS prior to use, following previously published purification protocols (Carvalho et al., 2015).

Behavioral assays

Defensive avoidance behaviors were assayed as before (Carvalho et al., 2015; Papes et al., 2010, 2018). Briefly, we used individually caged mice, which were habituated for 2 days to a dark room, where they were exposed on the following day to the amounts of stimuli listed on Table S1. Each stimulus was introduced on one side of the home cage and mice were filmed for 30 min with night-vision camera. All behaviors were visually scored blindly for avoidance time (Papes et al., 2010) – defined as amount of time spent more than 20 cm away from the odor source – and approach time, a measure of olfactory investigation, defined as the amount of time the animal spends clearly on top of or sniffing the odor source or within 1 cm from the stimulus in the cage.

Immunostaining procedures

c-Fos immunostaining was performed as previously described (Carvalho et al., 2015). Briefly, individually caged animals were habituated for 2 h during 2 days to a dark exposure room. On the following day, stimulus was introduced on one side of the home cage and exposure proceeded for 30 min, prior to stimulus removal. Animals were allowed a 60 min rest period without stimulation prior to being euthanized. Brains were dissected and fixed overnight in 4% paraformaldehyde (PFA). Fixed brains were equilibrated in sucrose and sectioned on a Leica 1000S vibratome to obtain 40 μ m sections. Blocking was done with 1% blocking reagent (Invitrogen), and all antibody incubations were performed in 1% BSA/1x PBS/0.3% Triton X-100, with washes in 1x PBS/0.1% Triton X-100 between incubation steps. Antibodies were anti-c-Fos rabbit polyclonal (Ab5; Millipore; 1:1500), anti-c-Fos goat polyclonal (Santa Cruz Biotechnology Sc-52 g; 1:500), anti-ER α (estrogen receptor alpha; Santa Cruz Biotechnology Sc-542; 1:500), and anti-SF1 (Transgene; 1:500). Sections were stained with DAPI nuclear stain and mounted onto microscope slides with ProLong Gold (Invitrogen). Dry mounted sections were imaged on a Nikon A1 or on a Leica TCS SPE confocal fluorescence microscopes.

For quantifying the spatial location of c-Fos-positive cells in the VMH, the nucleus' dorsomedial, dorsal and ventral boundaries were recognized after DAPI nuclear staining. These margins are easily observable due to the high cell density in the VMH near these boundaries, clearly different from the sparser surrounding areas (between the VMH and DMH, and between the VMH and Arc). Next, a delimiting oval was placed on top of the image, aligning its dorsomedial, dorsal and ventral margins to the boundaries recognized in the stained image. The dorsomedial-ventrolateral long x axis of the oval had approximately 430 μ m in length, and the perpendicular short y axis of the oval had approximately 240 μ m in length. Next, the coordinate of each c-Fos positive stained nucleus in the section was recorded along the x axis. Numbers of cells falling into each of 5 subdivisions running for intervals of 100 μ m along the x axis were computed and plotted as bar graphs in Figures 1J and S1A. Additionally, the positions of all stained cells across 6 animals were represented in a pooled fashion in the ovals in Figures 1J and S1A, with the interquartile range and distribution extremes represented in the box-whisker bars, both along the dorsomedial-ventrolateral x axis and along the perpendicular axis, having the centroid of the distribution (median values) in both axes at its center. This procedure does not account for small differences in VMH size and shape at bregma – 1.46mm and some c-Fos-positive cells near the margins or toward the more undefined ventrolateral border were inevitably

left out of the delimiting oval, but this standardized procedure allowed us to compare the spatial locations between activated ensembles with more parsimony than arbitrarily free-drawing the nucleus' boundaries (as depicted in [Figures 1A–1H](#), for example).

In situ hybridization and dual staining

For VNO activity analyses, some experiments ([Figures S4B and S4C](#)) analyzed the expression of the surrogate marker of vomeronasal activity *Egr1* ([Isogai et al., 2011](#)) combined with detection of *Vmn2r* receptor genes (coding for V2R family receptors) by *in situ* hybridization (details on probe validation are found in [Carvalho et al. \[2015\]](#)). Animals were exposed to the stimulus, according to quantities listed on [Table S1](#), for 45 min prior to euthanasia, VNO dissection and fixation by immersion in 4% paraformaldehyde overnight. Sixteen micrometer cryostat VNO sections were dried for 10 min, fixed in 4% paraformaldehyde, and acetylated in 0.1M triethanolamine (pH 8.0) / acetic anhydride. Hybridization with *Vmn2r* and *Egr1* gene probes was performed overnight using ~1,000 nt DIG- and DNP-labeled cRNA fragments, respectively (1,500 ng/mL each), at 58°C in 50% formamide, 10% dextran sulfate, 600mM NaCl, 200 µg/ml yeast's tRNA, 0.25% SDS, 10mM Tris-HCl pH8.0, 1X Denhardt's, 1mM EDTA pH 8.0. After stringent washes in 2x SSC, 0.2x SSC and 0.1x SSC (30 min each), sections were incubated with 0.1% Tween-20 for 10 min, and blocked in 100mM Tris-HCl pH 7.5, 150mM NaCl, 0.05% blocking reagent (Perkin Elmer). Anti-DIG (Roche; 1:500) or anti-DNP (Thermo Scientific; 1:600) were used to detect the probes. For each, we applied two steps of signal amplification with the tyramide signal amplification kit (Perkin Elmer), with steps in tyramide-biotin (1:50; Perkin Elmer), streptavidin-HRP (1:100), and tyramide-Alexa 488 or Alexa 555 (1:100 in 0.0015% H₂O₂ (Life technologies)). HRP (peroxidase) was inactivated between labeling steps by treatment with 3% H₂O₂ for 1h.

For experiments combining *in situ* hybridization of *Vmn2r* probes with pS6 immunostaining, after the cRNA hybridization and detection steps, sections were incubated in 3% H₂O₂ for 1 h, 0.1M HCl for 15 min, followed by an extra blocking step with 1% blocking reagent (Invitrogen), incubation with anti-phosphorylated ribosomal protein S6 rabbit polyclonal (Ser244, Ser247 anti-pS6; Thermo; 44-923G; 1:200; [Knight et al., 2012](#)) in 1% BSA/1x PBS/0.3% Triton X-100, and SuperBoost signal amplification with POD-conjugated secondary antibody (1:100 for 1h) and tyramide-Alexa-546 (1:50; Life Technologies) for 15 min. DAPI staining and mounting in ProLong Gold were performed as before.

Vmn2r (V2R) probes for the following genes were used: *Vmn2r13* and *Vmn2r89* for clade A1; *Vmn2r116* for clade A3; *Vmn2r28* and *Vmn2r41* for clade A4; *Vmn2r69* for clade A5; *Vmn2r90*, *Vmn2r107*, and *Vmn2r58* for clade A8; *Vmn2r20* for clade B; *Vmn2r56* for clade D (nomenclature following previously published clade distribution of V2R vomeronasal receptors) ([Silvotti et al., 2007](#)).

For the dual c-Fos immunostaining / *in situ* hybridization experiments in [Figures 2 and S1](#), we followed our previously described protocol ([Carvalho et al., 2015](#)). Briefly, half of the soiled bedding from the individually caged animal was transferred to a second cage, and the animal was exposed in its home cage for 20 min with snake odors. Next, the mouse was transferred to the second cage and left unstimulated for 1 h, and then stimulated with cat odors for an additional 20 min. Animals were sacrificed and perfused with 4% PFA and the dissected brains were sectioned to obtain 40 µm sections on a VT100S vibratome (Leica). Sections at the indicated bregma values for VMH were used to detect c-Fos mRNA and protein indicative of the second and first activation periods, respectively. Details on the dual staining and validation of this method based on the catFISH procedure ([Guzowski et al., 1999, 2001](#); [Lin et al., 2011](#)) can be found in our previous paper ([Carvalho et al., 2015](#)). It is important to mention that the time between both stimulation periods is sufficiently long to allow us to parse out the c-Fos mRNA indicative of activation during the last exposure and the c-Fos protein is indicative of the first exposure (note that no mRNA from the first exposure remains after 80 min and little c-Fos protein is synthesized to high levels from the second exposure in [Figures S1F and S1G](#)). The longer separation between the two stimulation windows (each is 20 min long and separated by 60 min) was previously tested and seen to be ideal to allow good temporal resolution in detecting c-Fos protein and mRNA. It should be noted that the number of c-Fos stained cells appears smaller in this protocol when compared to the regular immunostaining in [Figures 1A and 1F](#) due to the following reasons: (a) the c-Fos protein is detected 100 min after the onset of the first stimulation, which is longer than the 90 min applied in regular c-Fos immunostaining protocols; (b) each olfactory stimulation window in the dual staining is 20 min long, shorter than the usual 30 min long exposure in regular c-Fos immunostaining.

For calculating the levels of overlap expected by chance between the green and red labeling in the dual protocol, we counted the total number of DAPI-stained nuclei for each imaged section (n), followed by the calculation of an expected value of overlap by chance (O_{exp}) considering that the green (g) and the red (r) subpopulations of cells for each section were spatially randomly dispersed throughout the nucleus. In brief, each cell in the total of n cells counted was assigned a serial number, g green cells were randomly positioned in the series, and r red cells were randomly positioned in the series, using R programming. The final red-green overlap was computed and the procedure was repeated 1,000 times, with the average representing O_{exp} for that section. The mean O_{exp} was calculated for all sections and compared to the observed overlap levels, using one-tailed Welch's t test assuming unequal variances, in order to verify whether the observed overlap is statistically significantly higher than the value expected by chance.

Viral tracing in FDC mice

In FDC mice, the destabilizing domain fused to Cre is a mutant *E. coli* dihydrofolate reductase (ecDHFR), which renders DD-Cre unstable and prone to proteasome degradation, unless ecDHFR inhibitor trimethoprim (TMP) is present. TMP is not toxic and is not known to activate any endogenous receptors or to produce any behavioral changes in mice ([Iwamoto et al., 2010](#); [Sando et al., 2013](#); [Tai et al., 2012](#)). Adult 2 to 4 months-old FDC sexually naive mice were anaesthetized with isoflurane (0.8%–5%), placed on

a stereotaxic frame (David Kopf Instruments) and microinjected with an AAV1.CAG.flex.tdTomato.WPRE.rBG vector in one hemisphere to target the VMH, using a pulled glass capillary (Picospritzer) at a flow rate of 30 nl min^{-1} . Stereotaxic injection coordinates to target the VMH were obtained from the Paxinos and Franklin atlas (AP: -1.45 , ML: ± 0.68 , DV: -5.75 mm). Virus-injected animals were individually housed for recovery during 2–4 weeks and then exposed to cat or snake stimuli for 30 min, as described in the Animals sub-section. Fifteen minutes after exposure, each animal was injected with TMP lactate ($150 \mu\text{g/g}$ of body weight), left undisturbed for 3h and returned to the vivarium for 2–4 weeks for tdTomato expression. Next, animals were euthanized and fixed brain sections were produced at bregma positions -3.40 and -0.82 for the histological analyses of the PAG and AHN nuclei, respectively, using the natural tdTomato fluorescence without any signal amplification. Confocal microscopy z series (25 to 30 images per stack) were collected on an A1 Nikon confocal microscope over $40 \mu\text{m}$. Each stack was analyzed on ImageJ to produce the maximum intensity projection, followed by normalization of color intensity to the same arbitrary level to uniformly remove background from all compared images. Nucleus and sub-nucleus areas were delimited using the Paxinos mouse brain atlas as a reference. Binary images were evaluated with the ‘analyze particles’ function on ImageJ, followed by summing up all particle areas and comparison to the whole nucleus/sub-nucleus area to determine pixel density. In [Figure 4F](#), each individual measurement (red or blue open circles) represents pixel density (nucleus area occupancy) normalized to a preset number of 100 tdTomato cell bodies in the VMH image collected from the same injected animal. In [Figure S4E](#), the number of tdTomato+ cell bodies was counted in a $300 \times 300 \mu\text{m}$ square aligned with the centroid of the spatial distribution of labeled cells in each VMH section, or near the ventral border of the DMH (closer to the VMH injection site), or immediately medial to the fornix in the LHA.

QUANTIFICATION AND STATISTICAL ANALYSIS

We used *R*, Stat, and GraphPad Prism 8 packages for statistical analyses, in which p values are the probability that the null hypothesis (means are equal) is true. For comparing mean pixel density in the AHN and PAG, we used Welch’s t test assuming unequal variances. All other experiments were analyzed with one-way Analysis of Variance (ANOVA), followed by Tukey-Kramer HSD post hoc test. Group sizes and p values are reported in the figure legends.

Cell Reports, Volume 32

Supplemental Information

Representation of Olfactory Information

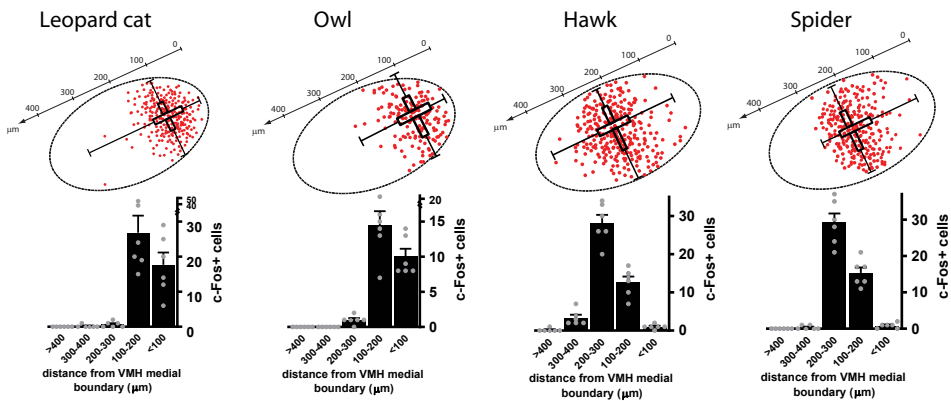
in Organized Active Neural

Ensembles in the Hypothalamus

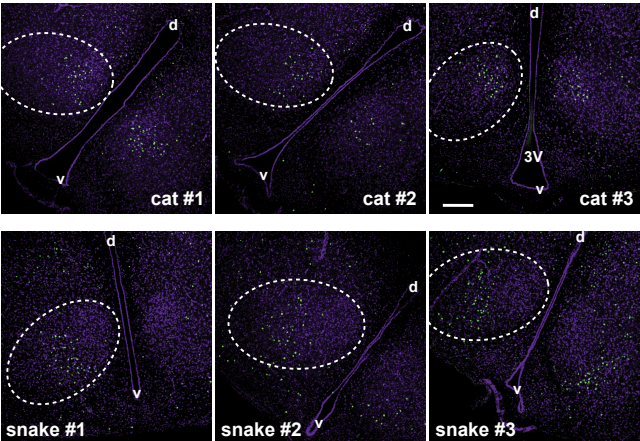
Vinicius Miessler de Andrade Carvalho, Thiago Seike Nakahara, Mateus Augusto de Andrade Souza, Leonardo Minete Cardozo, Guilherme Ziegler Trintinalia, Leonardo Granato Pissinato, José Otávio Venancio, Lisa Stowers, and Fabio Papes

Figure S1 - Carvalho et al., 2020

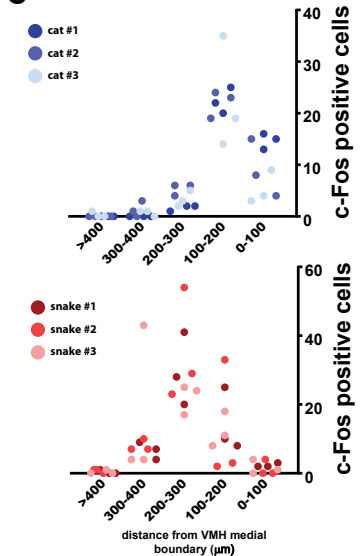
A



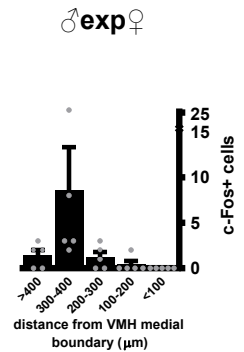
B



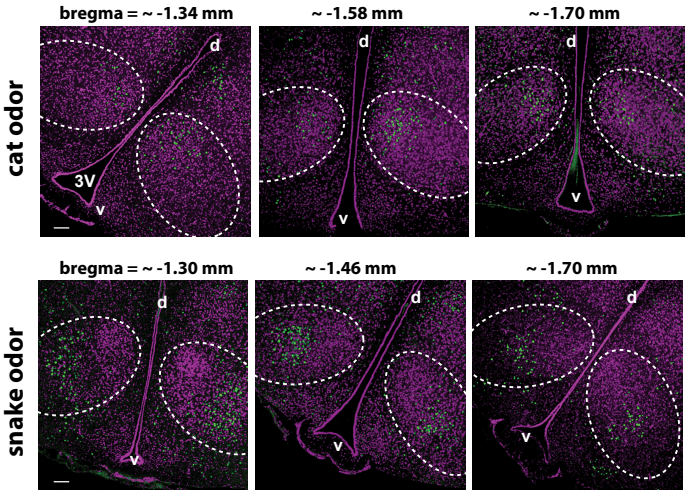
C



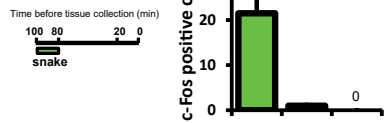
D



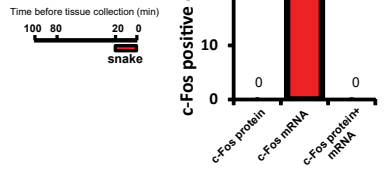
E



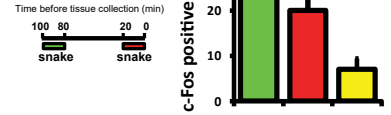
F



G



H



I

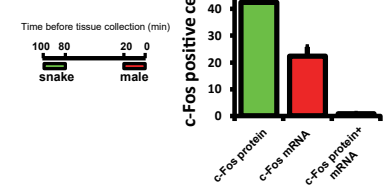


Figure S1. Experimental controls for VMH ensemble mapping and dual c-Fos immunostaining / *in situ* hybridization. Related to Figures 1 and 2.

- (A) VMH ensemble mapping and quantification for several olfactory stimuli (complementary to Figure 1K). See Figure 1 legend for details. Mean + SEM. n = 6 mice.
- (B) Exposure of mice to odors from different donor individuals yields similarly positioned active VMH ensembles.
- (C) Quantification of active ensembles in **B** in five 100 μ m wide zones along the VMH's dorsomedial-ventrolateral axis direction (see STAR Methods for details) for 3 individuals, represented by differently colored dots in the graphs.
- (D) Quantification of distribution of c-Fos+ cells in the five 100 μ m zones along the VMH's long axis in male mice exposed to female odors. Mean + SEM. n = 5 mice.
- (E) Location of c-Fos+ cells in animals exposed to cat (top) or snake (bottom) stimulus in sections at the different indicated bregma values. The image for VMH activation after exposure to snake stimulus in Figure 1F is a cropped version of this image, which shows both VMH nuclei at bregma - 1.46 mm.
- (F) Dual immunostaining / *in situ* hybridization to control for activity related to one exposure to olfactory stimulus during the first application window (100 to 80 min prior to brain fixation). Left: exposure protocol. Right: quantification of activated cells related to stimulus exposure. The first bar (green) represents cells activated in the first exposure only, the second bar (red) exhibits rare cells expressing c-Fos mRNA, and the third bar (yellow) represents very few cells expressing both nuclear c-Fos protein and mRNA. n = 4 animals.

(G) Same as in **F**, but to examine activated cells related to one exposure to stimulus during the second application window (20 to 0 min before brain fixation). Mean + SEM.

n = 4 animals.

(H) Dual staining control in animals exposed twice to the same stimulus (snake odor).

(I) Dual staining to show activity related to one exposure to snake stimulus and one exposure to conspecific stimulus (male mouse odors).

d, dorsal; v, ventral; 3V, third ventricle. Scale bar = 100 μ m.

Figure S2 - Carvalho et al., 2020

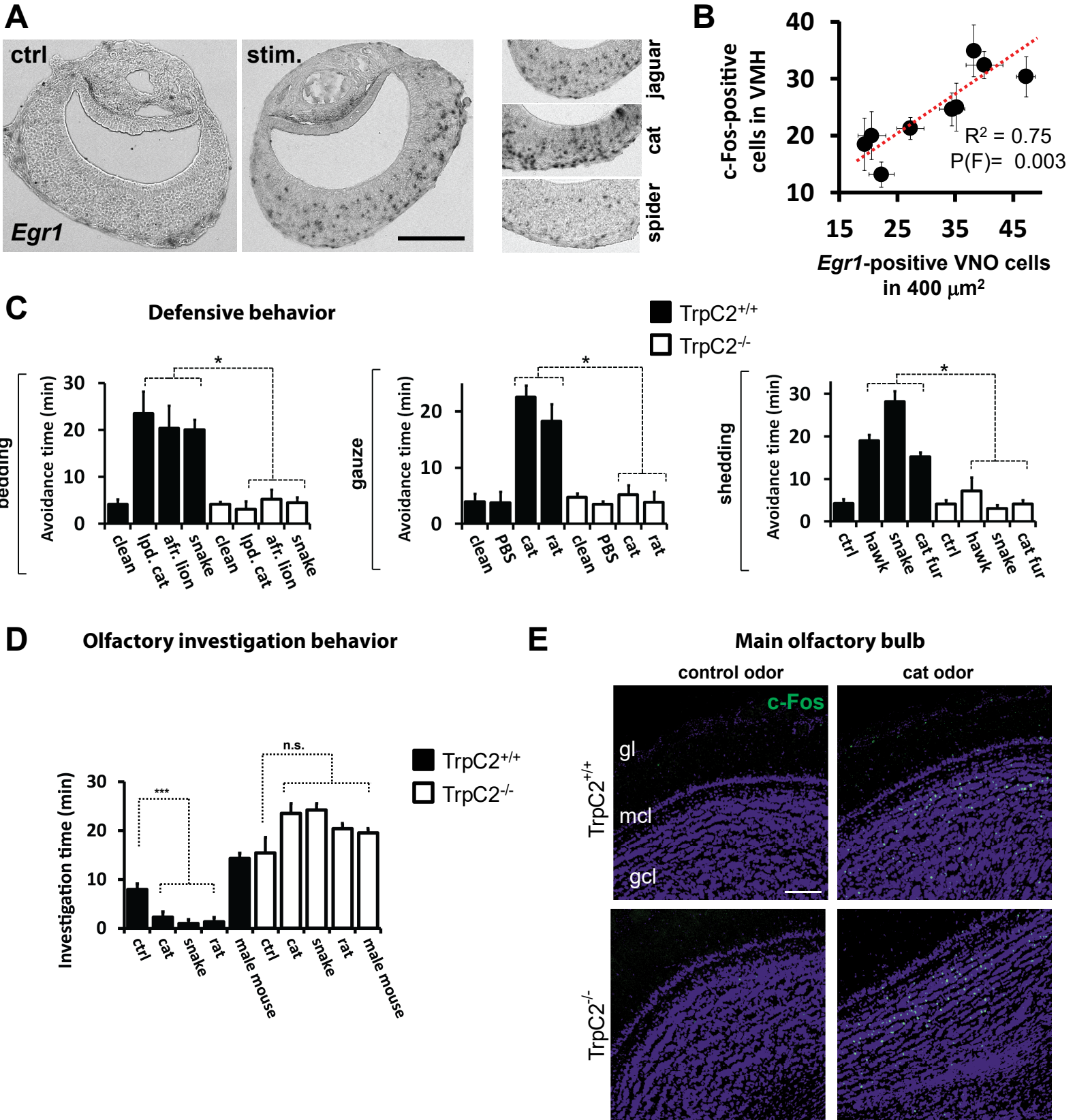


Figure S2. The VMH neural map is dependent on a functional VNO. Related to Figure 3.

(A) Exposure of male mice to chemical stimuli (stim.) activates VNO neurons, as evidenced by *in situ* hybridization to immediate early gene *Egr1*. Control (ctrl) odor is PBS-soaked gauze for liquid stimuli (similar number of *Egr1*-positive cells were found for other controls). Scale bar = 100 μm . lu, VNO lumen. Black labeling, *Egr1 in situ* hybridization signal.

(B) Scatter plots comparing the activation level in the VNO (judged by the number of nuclei expressing the immediate early gene *Egr1* in a 400 μm^2 area of sensory epithelium) and the activation level seen in the VMH, as judged by the number of c-Fos positive cells per unit area. The R^2 and probability values for the F statistics indicate the amount of variance explained by the linear regression model (dashed red line) and the likelihood that the data fit the model, respectively. Note the positive correlation between VMH activation and VNO activation. In the same animals, absence of correlation is observed in the piriform cortex (Carvalho et al., 2015), whose activation status reflects events in the main olfactory epithelium, not the VNO. Mean \pm SEM in both axes.

(C) Quantification of defensive avoidance behavior induced by most stimuli employed here, showing loss of behavior in *TrpC2*^{-/-} (white bars) compared to *TrpC2*^{+/+} (black bars) littermates. Behaviors are separated according to form of stimulus presentation (bedding, gauze, or shedding), with the corresponding appropriate unscented controls (clean or PBS). Mean \pm SEM. n = 8-12 animals. * P < 0.01; One-way ANOVA followed by HSD *post-hoc* test. lpd. cat, leopard cat; afr. lion, African lion.

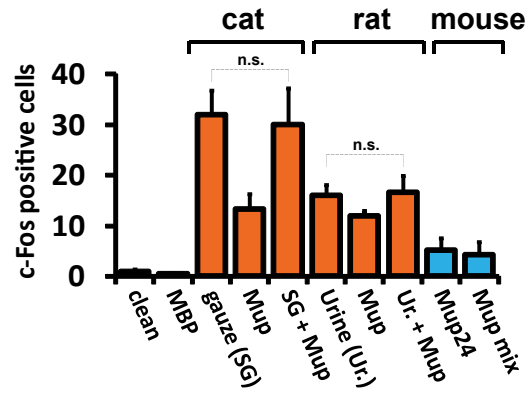
(D) Olfactory investigation behavior (approach time) in *TrpC2*^{+/+} (black bars) and

TrpC2^{-/-} (white bars) mice. Mean + SEM. n = 6-8 animals. n.s., non-statistically significant. ** P < 0.001; One-way ANOVA followed by HSD *post-hoc* test.

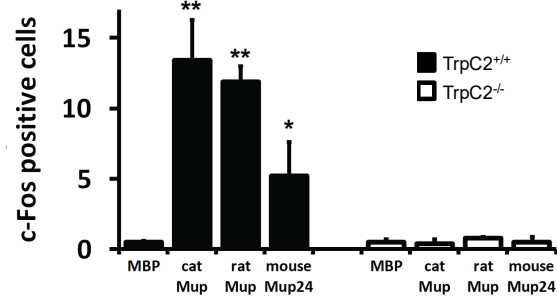
(E) c-Fos expression in the main olfactory bulb, an MOS-recipient brain area, for cat odor and respective control, in *TrpC2*^{+/+} and *TrpC2*^{-/-} mice. gl, glomerular layer; mcl, mitral cell layer; gcl, granule cell layer. Scale bar = 100 μm.

Figure S3 - Carvalho et al., 2020

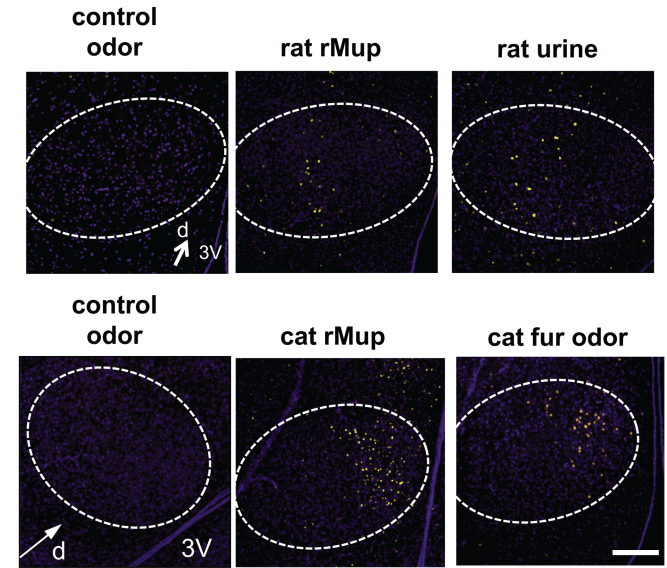
A



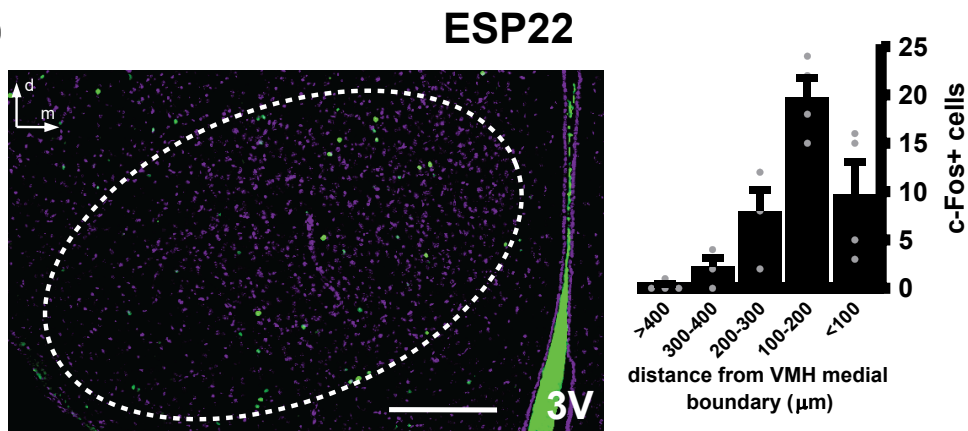
B



C



D



E

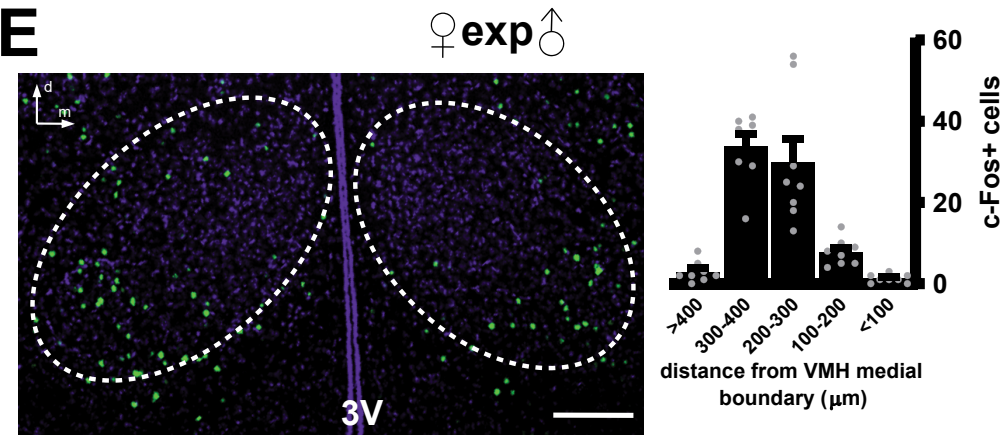


Figure S3. Supporting data for VMH activity induced by VNO stimuli. Related to Figure 3.

(A) Activity in the VMH in animals separately exposed to purified ligands presented in the same amount (cat, rat or mouse Mups). Mup24 or a mixture of Mup24, Mup3, Mup8 and Mup25 (Mup mix) were used at the same total amount. The number of c-Fos expressing cells is also shown for corresponding native stimuli, namely cat-scented gauze (SG) and rat urine (Ur.). Note that neural activity due to each pure recombinant Mup is contained within that induced by the corresponding native stimulus, because exposure to a combination of Mup along with its respective complex odor did not result in the summation of activities due to each separate stimulus. Heterospecific stimuli are indicated in orange and conspecific ones in blue. Clean gauze and gauze soaked with maltose binding protein (MBP) were used as unscented controls for liquid and solid stimuli, respectively. All recombinant Mup proteins are fusions with MBP. Mean + SEM. n = 8-12. ANOVA followed by Tukey-Kramer HSD *post-hoc* analysis. n.s., no statistically significant difference.

(B) Quantification of c-Fos⁺ cells in VMH in animals exposed to purified cat, rat and mouse Mup stimuli in *TrpC2^{+/+}* (black bars) and *TrpC2^{-/-}* (white bars) mice. Mean + SEM. n = 6. *P<0.01; **P<0.001; ANOVA followed by Tukey-Kramer HSD *post-hoc* analysis.

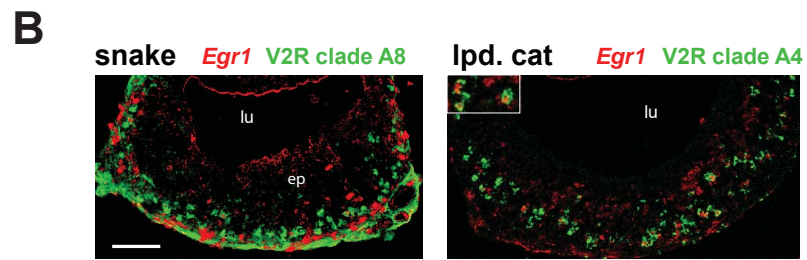
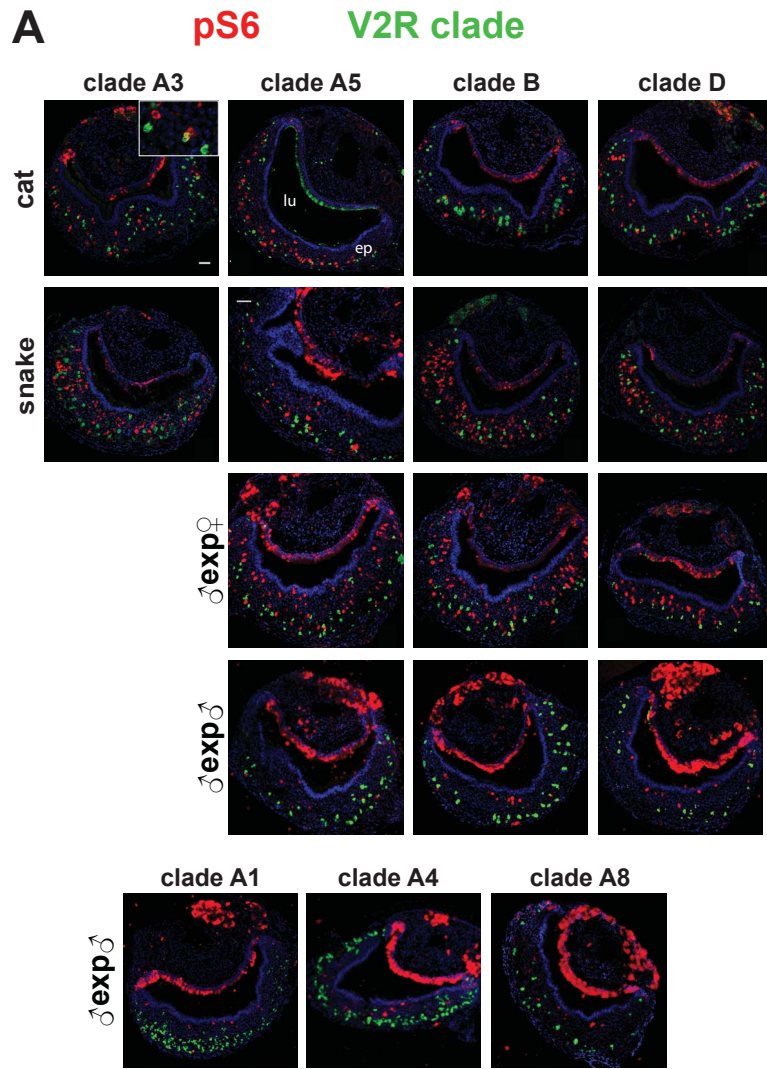
(C) Representative c-Fos staining (yellow) images from VMH of animals exposed to cat and rat purified Mup compared to the corresponding native stimulus. Note the similarly located active VMH ensemble for cognate pure and native stimuli. Nuclear staining in blue.

(D) Left, Representative c-Fos staining (green) image of male exposed to ESP22 peptide. Nuclear staining in purple. Right, Quantification of c-Fos staining in five 100 μm wide zones in VMH. Mean + SEM. n = 4 animals.

(E) Similar to D, but in female mice exposed to male odors. Mean + SEM. n = 8 animals.

d, dorsal; m, medial; 3V, third ventricle. Scale bar = 100 μm .

Figure S4 - Carvalho et al., 2020



C

V2R clade	no. receptors	cat	lpd. cat	mtn. lion	rat	owl	snake	ESP1	ESP22
A4	>30	■	■	■	■	■	■	■	■
A3	6							■	■
A5	15								
A1	18						■		
A8+A9	>30				■		■		

co-expression of *Egr1* and V2R clade

- > 10 cells
- 3-10 cells
- 1 or 2 cells
- no co-localization

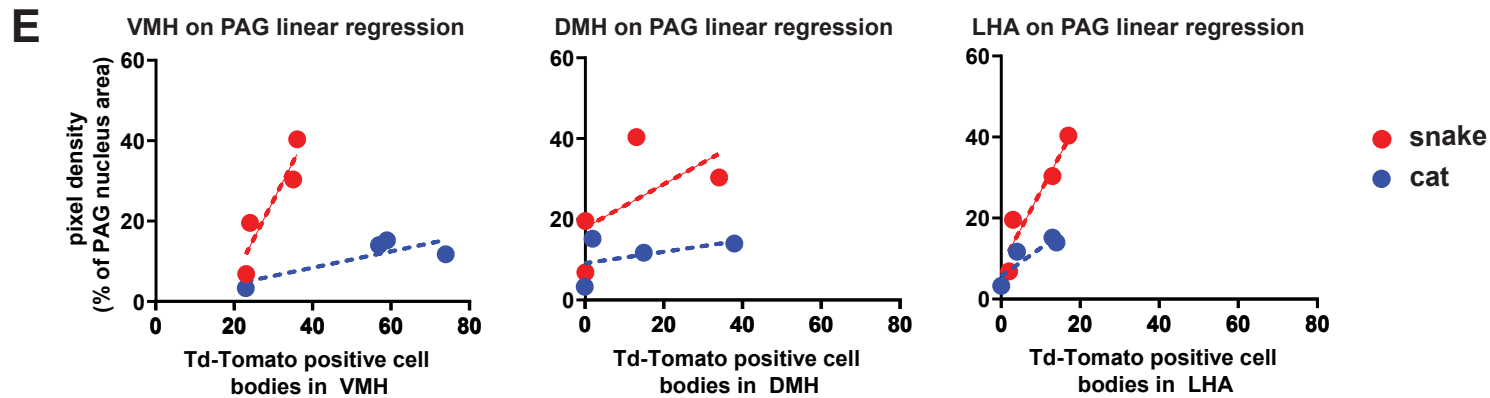
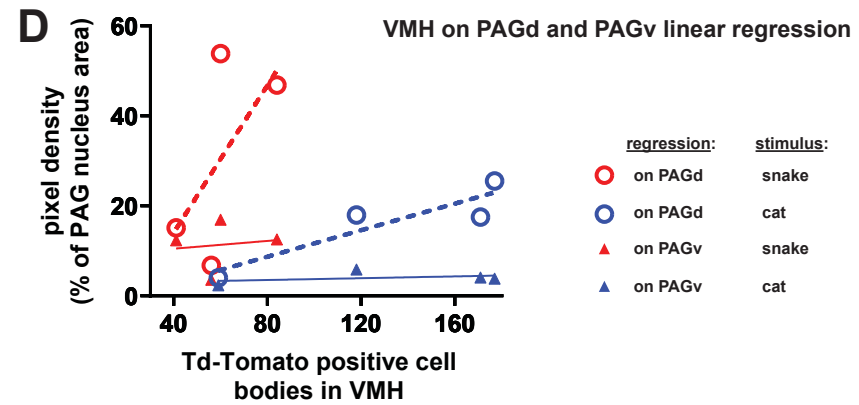


Figure S4. Additional pS6 and *Egr1* staining and controls for tracing experiments.

Related to Figures 3 and 4.

(A) Representative images of combined *in situ* hybridization for vomeronasal receptors (green) and immunostaining for vomeronasal activity marker pS6 (red) in VNO sections of animals exposed to different stimuli. Insets are higher magnification sectors of the image, to evidence presence or absence of labeling co-localization in each panel. For all stimuli, except males exposed to male odors, the results are for A3, B and D clades of V2R receptors. Clade C was not investigated, due to its widespread expression in the VNO epithelium. Results for males exposed to male odors show the complete set of V2R probes. Nuclear staining in blue.

(B) Examples of double *in situ* hybridization for *Egr1* (red) and vomeronasal receptors (green) in VNO sections of animals exposed to different stimuli, with labeling co-localization evidenced in inset. lu, lumen. Scale bar = 100 μ m. lpd. cat, leopard cat.

(C) Heat map showing V2R receptors in several clades expressed in VNO neurons activated after exposure to various heterospecific and conspecific stimuli. The number of receptors (no. receptors) in each clade is given in the second column. Dark blue indicates average co-expression of *Egr1* and the tested clade in more than 10 cells per VNO section. Intermediate blue hue indicates 3 to 10 co-labeled cells per section, lighter blue indicates 1 or 2 co-labeled cells per sections, and white indicates absence of co-labeling. n=10 sections. These V2R assignments are in accordance with other studies (Ferrero et al., 2013; Haga et al., 2010; Isogai et al., 2011). (Isogai et al., 2011) also contains information about V2R receptors expressed in cells activated by other stimuli. lpd. cat, leopard cat; mtn. lion, mountain lion.

(D) Correlation between number of tdTomato+ cell bodies in the VMH and normalized pixel density in PAG_d (open circles) and PAG_v (triangles), for snake (red symbols) and cat (blue) stimuli. Linear best-fit regression curves are shown for PAG_d (dashed lines) and PAG_v (continuous lines). n = 4 animals. See STAR Methods for details.

(E) Correlation between normalized pixel density in the PAG and the number of tdTomato+ cell bodies in a 0.09 mm² area of the VMH, DMH, and LHA nuclei.

lu, lumen; ep, sensory epithelium. Scale bar = 100 μm.

Table S1. List of olfactory stimuli used in the study. Related to Figures 1 and 2.

Common species donor name	Stimulus	Collection method	Control
Domestic cat	5 x 5 inches gauze	bodily scents collected by rubbing gauze against animal's fur	Unscented gauze
Leopard cat	50 ml solid scented bedding	directly collected from devoted cage	Clean bedding
African lion	50 ml solid scented bedding	directly collected from devoted cage	Clean bedding
Mountain lion	50 ml solid scented bedding	directly collected from devoted cage	Clean bedding
Rat	5 x 5 inches gauze scented with 1ml urine	urine collected with the help of a metabolic cage	Unscented gauze
Great horned owl	1 g of shed feathers, cut in small pieces	directly collected from devoted cage	Unscented gauze
Crested caracara hawk	1 g of shed feathers, cut in small pieces	directly collected from devoted cage	Unscented gauze
Jararaca snake	1 g of shed skin, cut in small pieces	directly collected from devoted cage	Unscented gauze
Tarantula spider	50 ml solid scented bedding (fine wood chips)	directly collected from devoted cage	Clean bedding
Mouse	50 ml of scented bedding (male) (fine wood chips)	directly collected from devoted cage	Clean bedding
Cat	10 mg of purified recombinant cat Feld4 Mup on gauze	purification as fusion with MBP	Gauze + 10 mg MBP
Rat	10 mg of purified recombinant rat Mup13 on gauze	purification as fusion with MBP	Gauze + 10 mg MBP
Mouse	10 mg of purified recombinant mouse Mup24 on gauze	purification as fusion with MBP	Gauze + 10 mg MBP
Mouse	10 mg of combined purified recombinant mouse Mups 24+8+3+25 on gauze	purification as fusion with MBP	Gauze + 10 mg MBP
ESP22	10 mg of purified recombinant juvenile mouse ESP22 peptide on gauze	purification as fusion with MBP	Gauze + 10 mg MBP